Reactivation of an errantivirus in *Drosophila* ovarian somatic tissue: from germline invasion to taming

Marianne Yoth[1], Stéphanie Maupetit-Méhouas[1], Abdou Akkouche[1], Nathalie Gueguen[1], Benjamin Bertin[2], Silke Jensen[1]*, Emilie Brasset[1]*

[1] iGReD, Université Clermont Auvergne, CNRS, INSERM, Faculté de Médecine, 63000 Clermont-Ferrand, France.

[2] LIMAGRAIN EUROPE, Centre de recherche, 63720 Chappes, France.

* Correspondence: emilie.brasset@uca.fr, silke.jensen@uca.fr

Summary

Most Drosophila transposable elements (TEs) are LTR retrotransposons, some of which belong to the genus Errantivirus and share structural and functional characteristics with vertebrate endogenous retroviruses (ERVs). These virus-derived elements occupy a large part of the genome, but it is unclear whether and how they can be reactivated and if they retain their replication capacity. We created conditions where control of the Drosophila *ZAM* errantivirus through the piRNA pathway was abolished leading to its reactivation in real time in somatic gonadal cells. We show that ZAM may remain active in these cells indicating that errantiviruses may hide from the efficient germline piRNA pathway by being expressed exclusively in somatic cells. After reactivation, *ZAM* invaded the oocytes and severe fertility defects were observed. The germline then set up its own adaptive genomic immune response against the constantly invading errantivirus, restricting invasion and restoring fertility. Our results not only highlight how errantiviruses and their host adapt to each other but also reveal a time window during oogenesis that may be favourable for viral germline invasion and endogenization.

Introduction

In vertebrates, many LTR retrotransposons belong to the family of endogenous retroviruses (ERVs). ERVs are a class of transposable elements (TEs) that are closely related to infectious retroviruses. Retroviruses are a family of RNA viruses defined by their ability to reverse transcribe their RNA genome into DNA which is then integrated into the host cell genome. While most retroviruses infect somatic cells, occasionally they may infect germ cells and if integrated in the germline genome, they may emerge as ERVs: they become permanent elements in the host genome and are vertically transmitted. ERVs are then capable of replicating themselves and integrating at new genomic loci, which contributes to their success in invading vertebrate genomes. In Human, ERV-related sequences occupy 9% of the genome, in mice 12%, in rat 10.2%, in microbats 5.3%, in marmosets 7.5% (http://repeatmasker.org/genomicDatasets/RMGenomicDatasets.html). Each new ERV copy then evolves independently and can be at the origin of the emergence of a new TE family. In mice, IAPE and IAP ERVs illustrate the evolutionary history of ERVs [1]. Indeed, IAPEs are still retroviruses capable of infecting other cells, after an extracellular passage, whereas the highly repeated IAPs, derived from IAPEs by losing the envelope gene (env), are strictly intracellular, evolving within a single cell.

It is crucial to note that TEs, can only be maintained in a species if they are able to transpose into the germline genome. If they do not, at least from time to time, they will accumulate mutations until there are no functional copies left and the TE family dies out. Some TEs gained cell and developmental stage specific expression [2–6]. TEs that have acquired the capacity to be expressed exclusively in somatic cells must therefore maintain their ability to invade germ cells to survive.

ERVs are TEs, and although the presence of TEs in the genome has been shown to provide some evolutionary benefits (reviewed in [7]), unregulated TE expression and transposition represent a threat to genome integrity and host fitness. Thus, under physiological conditions, most TEs are repressed by epigenetic mechanisms and maintained in a dormant state. In metazoan gonads, TE expression and mobilization is restrained by PIWI-interacting RNAs (piRNAs) (reviewed in [8,9]). The piRNA pathway has been extensively studied in the *Drosophila melanogaster* ovary that comprises about 16 ovarioles, each of which contains a succession of follicles composed of germ cells surrounded by somatic follicle cells [10] . piRNAs originate from specific source loci, the piRNA clusters [11]. In Drosophila, the piRNA clusters

expressed in the germline are particularly numerous and diverse while there is only one major piRNA cluster expressed in gonadal somatic cells, that is *flamenco* (*flam*) [12–16].

Within the Drosophila genome, there is a specific group of TEs that share structural and functional characteristics with vertebrate ERVs. These insect LTR transposons are classified as errantiviruses and belong to the Metaviridae family. In *Drosophila melanogaster* some errantiviruses have been shown to have the capacity to move from cell to cell. These include TEs such as *ZAM, Idefix* or *Gypsy* whose expression is restricted to the somatic follicle cells of the ovary [17–24].The intercellular invasion capacity may pose a particular threat, especially if they are able to cross the so-called Weismann barrier separating somatic and germ cells (reviewed in [25]). In the germ cells, TE expression and transposition are known to be controlled by the piRNA pathway, but research has primarily concentrated on how piRNAs silence TEs that are expressed in the cells where the corresponding piRNAs are produced. The role of piRNAs in the silencing of a TE that is activated in a cell type different from the one where the silencing mechanism must take place remains unclear. Consequently, whether these TEs can escape the robust epigenetic control mediated by piRNAs when arriving in the germline and how they are tamed by the host over time remained to be puzzled out.

The *ZAM* errantivirus was discovered through its uncontrolled activity in an unstable line, RevI-H2, about 25 years ago [26,27]. *ZAM* has 3 intact ORFs encoding proteins whose function is analogous to that of the Gag, Pol and Env proteins of ERVs or retroviruses [26]. In the RevI-H2 Drosophila line bearing a large deletion in the *flamenco* piRNA cluster, *ZAM* had become active and is specifically expressed in gonadal somatic cells [14,17]. Moreover, *ZAM* inserted into multiple new loci in the RevI-H2 line, including a germline-specific piRNA cluster, resulting in unexpected production of germline piRNAs that map to *ZAM* [26–28]. The biological role of these germline *ZAM*-mapping piRNAs remained unexplored.

Since these studies, *ZAM* has emerged as a key model for studying host-TE interactions and the relationship between somatic cells and the germline during TE invasion.

By analyzing different conditions of *ZAM* reactivation, we aimed here to study what happens in real time when an errantivirus is reactivated *de novo* and how the host responds. Specifically, we sought to elucidate whether piRNAs produced in the germline counteract TE invasion from the somatic cells or whether TE transcripts are protected from degradation by virus-like particles when arriving in the germline.

98 We show that in the RevI-H2 line, *ZAM* is still expressed in the follicle cells but it doesn't
99 invade the germline while *ZAM* copies with invasive capacities have been maintained in the
100 genome. To recreate the initial unstable condition, we *de novo* reactivated *ZAM* in the ovarian
101 follicle cells, either by soma-specific knock-down of the piRNA pathway, or by deleting a *ZAM*
102 copy in the somatic *flamenco* piRNA cluster, while keeping the piRNA pathway fully
103 functional. *De novo ZAM* reactivation in the follicle cells led to a massive *ZAM* invasion deep
104 into the adjacent oocyte and its ooplasm. We demonstrate that this invasion could be impeded
105 by the expression of *de novo ZAM*-targeting piRNAs produced in the germ cells themselves
106 demonstrating that these piRNAs are functional against the native *ZAM*. These results show
107 that by being expressed exclusively in somatic cells, errantiviruses may evade the control by
108 the very efficient germinal piRNA pathway and remain active for long periods of time. The
109 challenged germ cells then mount an adaptive genomic immune response to tackle the
110 permanent invasion.
111
112
113 # Results
114
115 **In an ancient *flamenco* mutant line, ZAM is still expressed, but the line is nevertheless**
116 **stable.**
117 To investigate the history of *ZAM* transposition dynamics, we monitored *ZAM* copies in the
118 RevI-H2i2 line, an isogenic line that was recently derived from the parental flam mutant RevI-
119 H2 line that has more than 25 years of laboratory history. It had previously been reported that
120 the RevI-H2 line was unstable and that *ZAM* actively transposed in this line [27]. The *ZAM*
121 instability in RevI-H2 had been linked to a deletion of a large part of the *flam* piRNA cluster.
122 This deletion spanned over more than 120 kb and comprised many different TE relics, including
123 more or less recent copies, and all *ZAM*-related copies of the *flam* locus [14,15].
124 In the RevI-H2i2 genome, Oxford Nanopore Technology (ONT) genome sequencing revealed
125 18 *ZAM* copies (Fig. 1a and Table 1 for coordinates). Only one of these *ZAM* copies was also
126 present in the reference genome (http://flybase.org). The other 17 new insertions were very

127 similar to the *ZAM* reference element identified in the initial RevI-H2 line [26] and we could
128 clearly localize 14 of the 17 new *ZAM* insertions. Interestingly, ONT long-read sequencing,
129 allowed identifying different *ZAM* variants. Specifically, six were full-length *ZAM* elements
130 (ZAM-fl), one, named *ZAM-v1,* harbored a deleted 5'-UTR (5' untranslated region), two, named
131 *ZAM-v3*, had a 303 bp deletion within the 5'-UTR, four had large internal deletions in the
132 coding regions, and four were full-length insertions with a deletion at the C-terminal end of the
133 *pol* gene of positions 5494 to 6120 in the *ZAM* internal sequence [26] (Repbase *ZAM*_I,
134 https://www.girinst.org/repbase/[29]). This deleted part of the *pol* gene does not correspond to
135 any known protein domain and the fact that there are five identical copies of this *ZAM* at
136 different locations in the RevI-H2i2 genome indicates that this *ZAM* variant, which we named
137 *ZAM-v2*, is competent for transposition. The full-length *ZAM*, *ZAM-v1* and *ZAM-v3* copies all
138 potentially encode Gag, Pol and Env proteins (Fig. 1a).
139 In the initial RevI-H2 line, a *ZAM* insertion was found in the germline piRNA cluster *9*, which
140 is close to the X chromosome centromere [28]. Here, in the RevI-H2i2 line, thanks to long-read
141 sequencing, we could identify *ZAM* insertions in repeated sequences, such as piRNA clusters,
142 more accurately. We now identified three *ZAM* insertions in piRNA cluster *9* (one *ZAM-fl* and
143 two *ZAM-v2*), and also a *ZAM-fl* insertion, which is localized in either piRNA cluster *13* or
144 cluster *56* (uncertainty is due to flanking repeats, piRNA clusters as in [30]) (Fig. 1a). We
145 reanalyzed the Illumina sequencing data of the initial RevI-H2 line and found evidence that all
146 these *ZAM* insertions in piRNA cluster 9 and 13 or 56 were already present ten years ago, and
147 that at least 14 of the *ZAM* insertions in the RevI-H2i2 line were already present in the parental
148 RevI-H2 line. This result indicates that the genomic *ZAM* profile is the same as ten years ago
149 and suggests that no new *ZAM* insertions occurred since then in the germline.
150 Strikingly, no new *ZAM* insertion was detected in the *flam* piRNA cluster. Thus, in the RevI-
151 H2i2 line, no *ZAM* piRNA can be produced from *flam*, the major somatic piRNA source locus.

152 Interestingly, single-molecule RNA fluorescence *in situ* hybridization (smRNA FISH) revealed
153 the presence of *ZAM* RNA in RevI-H2i2 follicle cells, demonstrating that *ZAM* is not silenced
154 in these somatic cells and that transcriptionally active copies of *ZAM* are still present in the
155 genome. *ZAM* transcripts were produced in follicle cells, starting very early during oogenesis
156 in the germarium. Then, after stage 8, *ZAM* transcripts accumulated in a patch of follicle cells
157 located at the posterior side of the follicles. We did not detect any *ZAM* staining in germ cells
158 (nurse cells or oocytes) (Fig. 1b). RNase A treatment led to complete loss of *ZAM* staining in
159 the follicle cells (Supplementary Fig. 1a). We did not detect any *ZAM* RNA in the Iso1A, w^{1118}
160 and w^{IR6} control ovaries (Supplementary Fig. 1b). Using RT-qPCR, we confirmed that *ZAM*
161 was expressed in the RevI-H2i2 ovaries. Conversely, other TEs such as the soma-specific *Gypsy*
162 and the germline-specific *Burdock*, were not upregulated (Fig. 1c). Interestingly, we observed
163 that, besides the full-length ZAM, at least *ZAM* variants ZAM-v2 and ZAM-v3 are expressed
164 in RevI-H2i2 ovaries (Supplementary Fig. 1c,d). *ZAM* is an errantivirus that encodes Gag, Pol
165 and Env proteins. Using immunostaining, we were able to detect *ZAM* Gag and Env proteins
166 that accumulated in the posterior follicle cells in late-stage follicles (> stage 9) (Fig. 1d). All
167 these results showed that *ZAM* transcripts and proteins are still expressed in the RevI-H2i2 line.
168 Although *ZAM* was expressed in follicle cells, the RevI-H2i2 line was fertile. Indeed, the ovary
169 morphology and the number of eggs laid were comparable in RevI-H2i2 and control females
170 (Fig. 1e, f). Altogether, these results indicate that no silencing mechanism had been set up to
171 repress the *ZAM* errantivirus in follicle cells suggesting that *ZAM* expression has no major
172 deleterious effect in the RevI-H2i2 line and that there is no selective pressure to specifically
173 repress *ZAM* in the follicles cells. These findings suggest that RevI-H2i2 is a stable line
174 although *ZAM* is actively expressed in follicle cells.
175
176 **Germline *ZAM*-targeting piRNAs constrain *ZAM* invasion from adjacent somatic cells.**

177 Transposition of *ZAM* in the initial RevI-H2 line had occurred in the germline, as attested by
178 the transmission of *ZAM* insertions to the offspring, despite the fact that *ZAM* is specifically
179 and exclusively expressed in the somatic follicle cells. This confirms that the *ZAM* errantivirus,
180 when expressed in follicle cells, transits to the germline to integrate into the germ cell genome.
181 However, we showed that *ZAM* insertions are stabilized in the RevI-H2i2 line. The RevI-H2i2
182 flies produce high amounts of sense and antisense *ZAM*-derived piRNAs with a ping-pong
183 signature, revealed by an over-representation of 10-nucleotide 5'-overlaps between sense and
184 antisense *ZAM*-derived piRNAs (Fig. 2a), while there was no ping-pong signature for ZAM in
185 diverse control lines [23,28]. Ping-pong amplification of piRNAs can only occur in the germline
186 in Drosophila (reviewed in [31]). Thus, these *ZAM* piRNAs observed in RevI-H2i2 are derived
187 from the germline. Importantly, our previous research has demonstrated that the X chromosome
188 of the RevI-H2 line, which contains the *ZAM* copies inserted in germline piRNA clusters, is
189 both necessary and sufficient to produce *ZAM*-regulating piRNAs [28]. Additionally, in both
190 RevI-H2 [28] and RevI-H2i2 background, a *ZAM* sensor transgene is silenced in the germ cells
191 (Supplementary Fig. 2a). We therefore hypothesized that piRNAs produced in germ cells can
192 thwart *ZAM* invasion from somatic cells to the germline and thus protect the germline from new
193 *ZAM* transposition. However, piRNAs are known to silence TEs in the cells where they are
194 produced and TEs, such as *ZAM*, are not expressed directly in germ cells but arrive from
195 surrounding somatic cells. Moreover, *ZAM* RNA may transit in an encapsulated form and the
196 capacity of piRNAs to target encapsulated RNAs remains unknown.
197 To test whether germline ZAM-derived piRNAs were efficient to counteract an invasion
198 coming from surrounding somatic cells, we abolished the piRNA pathway in the germ cells by
199 germline-specific knock-down (GLKD) of piRNA pathway components, in a RevI-H2i2
200 genetic background producing *ZAM* piRNAs in the germline. It is important to note that, during
201 the genetic crosses performed, only the X chromosome of the RevI-H2i2 was tracked to ensure

202 that the ZAM insertions in the germline piRNA clusters were maintained (crossing schemes
203 presented in Figure S6). We observed that the germline knock-down of proteins of the piRNA
204 pathway, Zucchini (Zuc), Argonaute 3 (Ago3) and Piwi, led to a decrease in the production of
205 *ZAM*-targeting piRNAs, i.e. piRNAs that are complementary and thus antisense to ZAM (Fig.
206 2b, Supplementary Fig.2b). The decrease in antisense piRNAs was comparable to that observed
207 for germline TEs (i.e., *Burdock* and *Accord*) or intermediate TEs (i.e., *Idefix*), while somatic-
208 TEs such as *Tirant* did not show a similar decrease. Furthermore, in *ago3*-GLKD ovaries, the
209 ping-pong signature for *ZAM* was abolished, as for many other germline-specific TEs, while it
210 was maintained in *piwi*-GLKD ovaries for instance (Fig. 2c, Supplementary Fig. 2c).
211 We then analyzed the subcellular localization of *ZAM* RNAs by smRNA FISH in the RevI-
212 H2i2 *white*-GLKD control line in which *ZAM*-derived piRNAs are produced in the germline.
213 *ZAM* RNA staining was restricted to follicle cells, only a minor *ZAM* RNA signal was detected
214 in the posterior pole of approximately 10% of stage 10 oocytes (Fig. 2d,e). However, when the
215 piRNA pathway was abolished in RevI-H2i2 germ cells through *vreteno (vret)*, *zuc, ago3* or
216 *armitage (armi) GLKD, ZAM* RNA was no longer restricted to follicle cells, a high signal was
217 also detected in oocytes. *ZAM* RNA spread throughout the ooplasm, but was clearly enriched
218 at the posterior pole of the oocyte, adjacent to the *ZAM*-expressing follicle cells, supporting the
219 fact that *ZAM* RNA originated from follicle cells (Fig. 2d). Actually, 30-70% of stage 10
220 follicles showed a strong *ZAM* RNA signal in oocytes (Fig. 2e). The strongest invasion
221 phenotype was observed for the RevI-H2i2 *ago3*-GLKD condition where we found a decrease
222 in the production of *ZAM*-derived piRNAs and the loss of the ping-pong signature (Fig. 2b). In
223 this condition, *ZAM* RNA accumulation in the ooplasm was correlated with a strong increase
224 of *ZAM* RNA in total ovaries (RT-qPCR data) (Supplementary Fig. 2d). These results showed
225 that when the piRNA pathway is affected in the germline, *ZAM* RNAs transit from the somatic
226 follicle cells, where they are produced, to the oocyte. Altogether, our data strongly suggest that

227 *ZAM* piRNAs produced by the germline piRNA pathway trigger post-transcriptional silencing
228 of *ZAM* RNAs arriving from follicle cells.
229 We confirmed this finding using a line where no *ZAM*-derived piRNA is produced in the
230 germline (w^{1118} genetic background) and in which we knocked down the piRNA pathway in the
231 follicle cells by somatic knock-down (sKD) of *armi*, *vret*, *piwi* or *yb*. The amount of antisense
232 piRNAs that target soma-specific TEs, including *ZAM,* was strongly decreased (Fig. 2f,
233 Supplementary Fig. 2e, f). RT-qPCR analysis showed that *ZAM* and another soma-specific TE,
234 *Gypsy*, were derepressed, but not the germline-specific *Burdock* (Supplementary Fig. 2g).
235 Importantly, smRNA FISH results revealed that *ZAM* RNAs were not restricted to the posterior
236 follicle cells. Like in ovaries harboring GLKD of the piRNA pathway in RevI-H2i2
237 background, *ZAM* RNAs were present in oocytes (Fig. 2g,h, Supplementary Fig. 2h). We
238 detected *ZAM* RNAs in the ooplasm in 90% of stage 10 follicles (Fig. 2i). This result confirmed
239 that, when no *ZAM* piRNA is produced in the germline, *ZAM* RNAs expressed in the somatic
240 follicle cells transit to the oocyte.
241
242 ***ZAM* RNAs transcribed in follicle cells transit to the oocyte and are conveyed to the**
243 **embryos in absence of germline ZAM piRNAs.**
244 Although *ZAM* is expected to be transcribed only in follicle cells due to its dependence on the
245 Pointed somatic transcription factor [17,32], it was possible that some ZAM copies acquired the
246 capacity to be expressed in the germline over time. Therefore, we wanted to rule out the
247 possibility that *ZAM* RNAs detected in the RevI-H2i2 oocyte originated from germinal nurse
248 cells. If some *ZAM* genomic insertions could be expressed in the germline of the RevI-H2i2
249 line, then germline depletion of *Piwi*, which is required for the transcriptional gene silencing of
250 TEs, should lead to the transcriptional de-silencing of *ZAM*. We observed that Piwi-GLKD in
251 the RevI-H2i2 ovaries led to the de-silencing of TEs that are capable of transcribing in the

252 germline such as *Burdock*. However, we did not observe any changes in either the *ZAM* RNA
253 level or localization (Fig. 3a,b). Moreover, depletion of *Ago3* induced a substantial
254 accumulation of *ZAM* RNA solely in the ooplasm. In contrast to TEs expressed in the germline
255 (e.g, *Burdock*), we never detected *ZAM* RNA staining in the cytoplasm of the nurse cells at any
256 stage (Fig. 3c). These results strongly support that *ZAM* cannot be expressed in the RevI-H2i2
257 germ cells and that *ZAM* RNAs detected in oocytes originate from the somatic follicle cells, not
258 nurse cells.
259 Throughout the animal kingdom, the first embryonic development stages are controlled by
260 transcripts and proteins deposited by the mother during oogenesis [33]. In Drosophila, most of the
261 maternal mRNAs are dumped from nurse cells into the oocyte during oogenesis. Although *ZAM*
262 transcripts originate from the somatic follicle cells, when we investigated *ZAM* RNA
263 transmission to the oocyte, we found such transcripts also in early embryos. Indeed, in
264 conditions where *ZAM* RNA had been detected in oocytes, smRNA FISH experiments revealed
265 a strong accumulation of *ZAM* RNAs in early embryos, before the zygotic transition, 0-2 hours
266 after egg laying: from a RevI-H2i2 mother with GLKD of the piRNA pathway, and also from
267 a mother without germinal *ZAM* piRNAs with sKD of the piRNA pathway in follicle cells (Fig.
268 3d, Supplementary Fig. 3a). Furthermore, *ZAM* RNAs accumulated at the posterior pole of early
269 embryos where future germ cells cellularize (Fig. 3e, Supplementary Fig.3b). We detected *ZAM*
270 RNA in high quantity until stage 5 of embryogenesis and few *ZAM* RNA signal persisting until
271 the cellularization of the blastoderm (~stage 8-9) (Fig. 3f). In the progeny of the RevI-H2i2
272 line, we did not detect any *ZAM* RNA, although *ZAM* RNAs were produced in follicle cells of
273 RevI-H2i2 ovaries (Fig. 3d). This confirmed that *ZAM* invasion of the germline does not occur
274 in this line. These data revealed an efficient post-transcriptional silencing of *ZAM* RNAs
275 arriving from follicle cells into the oocyte by piRNAs produced in the germline. This

276 mechanism should limit the transposition of the somatic *ZAM* retrotransposon into the germline
277 genome.
278
279 ***De novo ZAM* reactivation leads to massive oocyte invasion and may result in severe**
280 **fertility defects.**
281 Our results demonstrate that an adaptive response can emerge to counteract the invasion of
282 germ cells by an errantivirus. To go deeper, we sought to assess the direct impact of reactivating
283 an errantivirus in real time, before the establishment of any adaptive response by the germline.
284 To conduct this study, we aimed to specifically reactivate *ZAM de novo*. The loss of the piRNA
285 pathway in the somatic follicle cells leads to *ZAM* reactivation, however many other TEs are
286 also desilenced (Supplementary Fig. 2e, g). Moreover, alteration in the expression of piRNA
287 pathway genes also results in severe developmental defects during oogenesis [34–37]. Therefore,
288 this model cannot be used to specifically analyze the impact of *ZAM* reactivation in ovaries. On
289 the other hand, in the RevI-H2 line where *ZAM* was also reactivated, a large deletion of
290 *flamenco* occurred during non-targeted mutagenesis and an adaptive response had already been
291 set up in the germline. Thus, we chose to create a condition where a single TE is reactivated *de*
292 *novo* and the piRNA pathway is fully functional.
293 Using CRISPR-Cas9, we *de novo* deleted the longest *ZAM* copy in the *flam* piRNA cluster in a
294 line carrying the X chromosome of the Iso1A reference line. As in this line, the *flam ZAM* copy
295 is at the genomic position X:21,778,810..21,783,994, we used two guides designed to create a
296 deletion spanning over X:21,777,135..21,784,062 (6926 pb). We named the resulting line
297 *flamΔZAM*. Mapping of genome-unique piRNAs to the *flam* locus highlighted the complete
298 loss of piRNA production in the targeted region compared with the control Iso1A line (Fig. 4a).
299 Conversely, the global production of genome-unique piRNAs mapping upstream and
300 downstream of *ZAM* was not affected. We confirmed that the deletion induced a strong decrease

301 of all piRNAs mapping to the internal regions of the reference *ZAM*. However, piRNAs
302 targeting the *ZAM* LTR were still produced (Fig. 4b). In line with these results, PCR
303 amplification and DNA sequencing of the CRISPR-Cas9 target locus showed that only the
304 internal regions of *ZAM* had been deleted from the *flam* piRNA cluster, resulting in the retention
305 of a solo-LTR at the initial *ZAM* insertion site (Supplementary Fig. 4).
306 In the *flamΔZAM line*, only the production of *ZAM*-derived antisense piRNAs was strongly
307 altered, whereas the production of antisense piRNAs mapping to other TEs was not affected
308 (Fig. 4c). This shows that the *ZAM* deletion from *flam* impairs *ZAM*-derived piRNA production,
309 but does not affect the global piRNA production in ovaries. In sum, in the *flamΔZAM* line, the
310 piRNA pathway was functional and almost no piRNAs that could target the internal *ZAM*
311 sequences were produced.
312 We then analyzed *ZAM* RNA expression by smRNA FISH in *flamΔZAM* ovaries. Surprisingly,
313 we did not detect any *ZAM* expression (Fig. 4d- panel 1). Based on this observation, we
314 hypothesized that either there was no functional *ZAM* copy in the *flamΔZAM* line, or that the
315 *ZAM* solo-LTR retained in *flam* was sufficient to silence *ZAM* expression. To check this, we
316 exchanged chromosome II or III of the *flamΔZAM* line with chromosome II or III of the RevI-
317 H2i2 line that each contains three or two recently transposed potentially functional *ZAM* copies,
318 respectively. We made sure not to introduce the ZAM copies located in germline piRNA
319 clusters of the X chromosome of the RevI-H2i2 line that are involved in the production of
320 ZAM-regulating piRNAs in the germline. smRNA FISH revealed that *ZAM* RNAs were
321 strongly expressed when these *ZAM* copies were added to the genome of the *flamΔZAM* line
322 (Fig. 4d – panels 2 and 3). We also observed a strong invasion of oocytes with chromosome II,
323 where approximately 70% of stage 10 follicles presented *ZAM* RNAs in the ooplasm, and
324 moderate invasion with chromosome III. Similarly, we observed strong invasion of the oocyte
325 when we added three euchromatic *ZAM* copies located on the telomere side of the X

326 chromosome of the RevI-H2 line to the *flamΔZAM* genome (Fig. 4d – panel 4). Overall, our
327 findings show that in the absence of *ZAM*-derived piRNAs in the somatic follicle cells and in
328 the germline, transcripts from functional *ZAM* copies massively invade the oocytes.
329 Additionally, our results demonstrate that the presence of a solo-LTR of *ZAM* (454 bp) in the
330 *flam* piRNA cluster of the *flamΔZAM* line was not sufficient to silence *ZAM* expression in
331 follicle cells (Supplementary Fig. 4a). The three *ZAM* copies added to the X chromosome of
332 the *flamΔZAM* line consist of one full length *ZAM* insertion (*ZAM-fl*), one *ZAM-v2* and one
333 *ZAM-v3*. Utilizing the sequence specificity of each insertion, we conducted RT-PCR analysis
334 to determine which copies were expressed. The results revealed that *ZAM-fl*, *ZAM-v2* and *ZAM-*
335 *v3* copies are expressed in RevI-H2i2 ovaries as well as when joined to the *flamΔZAM* genome
336 (Supplementary Fig, 4b).
337
338 An important observation was that the *flamΔZAM* flies that contain the three functional *ZAM*
339 copies on the X chromosome displayed atrophied ovaries and reduced fertility compared with
340 the control *flamΔZAM* flies that lack functional *ZAM* copies (Fig. 4e,f). Specifically, 90% of
341 *flamΔZAM* females with active *ZAM* copies did not lay eggs. These data indicate that the
342 reactivation of one single errantivirus in a patch of follicle cells can induce severe fertility
343 defects. These results suggest that when *ZAM* piRNAs are produced in the germline, they
344 contribute to ensure not only genome integrity but also fertility by protecting the oocytes against
345 *ZAM* invasion.
346
347 **No initial small RNA response takes place after *ZAM* reactivation.**
348 The reactivation of an errantivirus, such as *ZAM,* in a genetic context where the piRNA pathway
349 is functional provides a unique opportunity to examine the genomic immune response to TE
350 reactivation and germline invasion. piRNAs and siRNAs are the two main classes of small

351 RNAs produced to control the expression of transposable elements and counteract viral
352 infection, respectively. Moreover, invading viral RNAs can be processed to small RNAs to
353 initiate a primary response [38,39]. To characterize the small RNA response upon *ZAM*
354 reactivation, we sequenced small RNAs that are complexed with Argonaute proteins (named
355 here "regulatory" piRNAs) from *flamΔZAM* ovaries containing two or four potentially
356 functional *ZAM* copies. In the *flamΔZAM* line, there were no *de novo ZAM* piRNAs (23 to 29
357 nt) produced upon *ZAM* reactivation, despite germline invasion. Indeed, only few sense and
358 antisense *ZAM* piRNAs were detected in the ovaries of the *flamΔZAM* line that contained
359 functional *ZAM* copies (Fig. 5a, Supplementary Fig. 5a). Moreover, this lack of piRNA
360 production concerned only *ZAM*. The level of regulatory piRNAs targeting other TEs was not
361 reduced (Fig. 5b, Supplementary Fig. 5b).
362 We sequenced total small RNAs in *vret*- or *yb*-sKD ovaries where *ZAM* was also reactivated.
363 Surprisingly we observed sense *ZAM*-mapping small RNAs of various sizes, including 23-29 nt
364 small RNAs that are not produced in a *white*-sKD control condition (Supplementary Fig. 5c).
365 However, the sense 23-29 nt *ZAM*-derived small RNAs detected in *yb*- and *vret*-sKD ovaries
366 did not display uridine bias at the 5' end, a feature of mature primary piRNAs (Supplementary
367 Fig. 5d). Furthermore, these sense *ZAM*-mapping small RNAs were not immunoprecipitated
368 with Piwi proteins. We detected almost no Piwi-bound sense or antisense *ZAM*-mapping
369 piRNAs in *vret*- or *yb*-sKD ovaries (Supplementary Fig. 5e). In addition, no sense regulatory
370 *ZAM* piRNAs complexed with Argonaute proteins were detected in *vret*-sKD ovaries
371 (Supplementary Fig. 2f). These results suggest that the sense *ZAM*-mapping small RNAs are
372 most likely degradation products of excess *ZAM* sense transcripts and not piRNAs. Thus, in
373 these different conditions, we did not detect any primary piRNA response either in the somatic
374 cells where *ZAM* is expressed or in the oocyte that it invades.
375

376 Given that the *ZAM* errantivirus shares some structural and functional characteristics with
377 retroviruses, we also asked whether *ZAM* reactivation could trigger a siRNA response. For this,
378 we analyzed the production of 21 nt small RNAs complexed with Argonaute proteins
379 ("regulatory" siRNAs). Similar levels of *ZAM* 21 nt small RNAs were produced in a control
380 line and in the *flamΔZAM* line with functional *ZAM* copies (Fig. 5c). Globally, the production
381 of 21 nt small RNAs in this line was comparable to the control for all TEs, including *ZAM* (Fig.
382 5d). *ZAM*-mapping 21 nt small RNAs were slightly increased only in the *vret*-sKD condition,
383 compared to the *white*-sKD control line without *ZAM* expression (Supplementary Fig. 5f).
384 Overall, our results suggest that no or very few siRNAs that could protect ovaries from *ZAM*
385 activity are produced upon activation of this errantivirus in follicle cells.
386 Therefore, we propose that no innate small RNA response is triggered in the lines where *ZAM*
387 is reactivated, suggesting that *ZAM* will not be brought under control until the establishment of
388 specific adaptive immunity and immune memory.
389
390

391 # Discussion

392 The discovery that piRNAs produced in germ cells not only restrict TE expression in the
393 germline itself but also counteract the invasion of errantiviruses from adjacent cells reveals a
394 novel role of piRNAs produced locally as an effective defense mechanism at the tissue scale.
395 When piRNAs against *ZAM* are produced in the germline, *ZAM* transcripts are limited to a patch
396 of follicle cells and flies are fertile. Conversely, in the absence of *ZAM*-derived piRNAs in the
397 germline, transcripts from functional *ZAM* copies massively invade the oocytes and are even
398 transmitted to the embryos. At the molecular level, our study revealed that piRNAs produced
399 in nurse cells and dumped into the oocyte can target RNAs produced by follicle cells and
400 delivered to the oocyte. It is tempting to speculate that the *ZAM* RNAs arriving from somatic

401 cells are targeted by complementary antisense piRNAs and degraded through the ping-pong
402 cycle (reviewed in [31]). This would result in the production of *ZAM* sense piRNAs, thus
403 participating in the amplification of the pool of piRNAs against *ZAM* and strengthening the
404 defense mechanism against the invasion.
405 Transposition in the germ cell genome is crucial for TE propagation in a population because it
406 allows the vertical transmission of new insertions. At the time of invasion (e.g. in the *flam*Δ*ZAM*
407 line), no *ZAM*-derived piRNA was produced in somatic or germ cells. Therefore, this condition
408 could be compared to what happens when a TE first enters a new species by horizontal transfer.
409 In this case, according to several studies, an initial transposition burst occurs that leads to TE
410 accumulation in the genome before the induction of an adaptive response by the host to control
411 transposition [40–45]. We found at least 17 new *ZAM* insertions in the RevI-H2i2 genome,
412 testifying that *ZAM* actively transposed. Surprisingly, we identified three *ZAM* insertions in the
413 same germline piRNA cluster on the X chromosome. It has been proposed that two different
414 mechanisms can explain the *de novo* piRNA production required to specifically silence a novel
415 invading TE. Indeed, piRNAs can be produced from a new TE insertion into a pre-existing
416 piRNA cluster, and also by stand-alone TE insertions converted into piRNA-producing loci [46–
417 49]. Interestingly, when active *ZAM* copies are added into a *flamΔZAM* genetic background, these
418 copies do not produce regulatory *ZAM*-derived piRNAs and are not converted into piRNA
419 producing regions. Actually, *ZAM* should be transcriptionally inactive in the germline because
420 *ZAM* expression is regulated by the somatic transcription factor Pointed [32]. Therefore, although
421 the contribution of individual copies needs to be investigated, our data strongly suggest that
422 germline *ZAM* piRNAs originate at least in part from piRNA clusters. In line with our findings,
423 computer simulations of the TE invasion dynamics suggested that several insertions in piRNA
424 clusters are likely to be required to stop the invasion in the germline [50] . Conversely, we found
425 that a single insertion in a somatic piRNA cluster, such as *flamenco,* is sufficient for TE

426 silencing in the somatic follicle cells, as previously suggested [14]. Indeed, we show here that in
427 follicle cells, the *flamenco* piRNA cluster acts alone as the principal regulator of transposon
428 activity. A precise deletion of the internal part of the *ZAM* TE inserted in *flamenco* leads to
429 complete derepression of functional *ZAM* copies. Surprisingly, it seems that reactivation of this
430 errantivirus in only a patch of somatic cells can lead to severe fertility defects. However, in the
431 germline, the deletion of the three most highly expressed germline piRNA clusters (42AB, 38C,
432 and 20A) affected neither fertility nor TE silencing [48]. This could be explained by the fact that
433 in the germline, but not in somatic cells, redundancy in piRNA production among different
434 piRNA clusters is observed, with probably multiple piRNA clusters involved in the silencing
435 of the same TE. Moreover, many TE copies have acquired mutations and are non-functional for
436 transcription or for transposition. In the *flam*Δ*ZAM* line, although no *ZAM* piRNA was
437 produced, we did not detect any *ZAM* expression. However, when we introduced functional
438 copies of *ZAM*, *ZAM* was expressed demonstrating that depending on the genetic background,
439 the transposon landscape varies and functional copies can be absent or present. In general, the
440 TE content varies considerably among populations [47,51]. Interestingly, we identified *ZAM* copies
441 with a deletion that affects the *pol* gene. The copy numbers of this *ZAM* variant *ZAM-v2* and of
442 *ZAM* full-length elements (ZAM-fl) that have transposed in the RevI-H2 line are similar (4 and
443 6 copies respectively), suggesting that even this *ZAM*-variant can transpose very efficiently.
444 Studies in different organisms have shown that TEs rapidly diversify. For instance, the *mariner*
445 DNA transposon is present in 68 different versions in grass genomes [52]. Such rapid
446 diversification certainly promotes speciation of new families of active TEs.
447 One interesting question is how *ZAM* RNAs transit into the oocyte and at which stage during
448 Drosophila oogenesis *ZAM* transposes in germ cells. We noticed that *ZAM* RNAs, although
449 transcribed in follicle cells, were deposited and accumulated at the posterior pole of early
450 embryos, where future germ cells cellularize. *ZAM* might have evolved to preferentially

451 mobilize in the dividing primordial germ cells of the offspring instead of the developing oocyte,
452 which is not in a phase favorable to transposition because of its prolonged arrest in prophase I
453 associated with highly compacted chromatin[53].
454 Previous experiments demonstrated that *ZAM* RNAs accumulate in follicle cells when
455 vitellogenesis is defective, suggesting that *ZAM* transmission to the oocytes requires functional
456 vitellogenin trafficking [20] (Supplementary Video 1). Moreover, errantiviruses, such as *ZAM*
457 and *Gypsy*, can form pseudo-viral particles in follicle cells when they are expressed [17,19,20,24].
458 *ZAM* Gag and Env proteins are expressed in RevI-H2i2 follicle cells. Retroviral envelope
459 glycoproteins undergo proteolytic processing by cellular serine endoproteases (furin and
460 proprotein convertases), in order to produce the two functional subunits, a glycosylated
461 hydrophilic polypeptide (SU) and a transmembrane domain (TM). This step is necessary to
462 achieve protein competence to promote membrane fusion and virus infectivity [54,55]. The
463 errantiviral *env* gene, acquired from insect baculovirus [56], encodes a protein whose function is
464 analogous to that of retroviral Env protein, which is responsible for infectious properties.
465 Indeed, *ZAM* Env protein is composed of an SU, a TM and an Arg–X–Lys–Arg conserved
466 domain, which is considered to be a furin consensus proteolytic cleavage site [26,55,57]. A recent
467 study demonstrated that intracellular retrotransposition of the *Gypsy* errantivirus can occur in
468 the absence of the Env protein, while intercellular transmission requires a functional Env [19].
469 Currently, whether *ZAM* can transpose intracellularly, in follicle cells, and the exact
470 mechanisms (Env protein dependent or independent) used for *ZAM* transmission to the oocyte
471 are unknown.
472 Once a virus enters the target cells, several scenarios for retrovirus uncoating have been
473 proposed. Recent advances on the HIV-1 strongly suggest an uncoating at the nuclear pore and
474 within the nuclear compartment [58]. Errantiviruses also encode Gag proteins which are capable
475 of mediating the assembly of virus-like particles. However, there are significant differences

476 between these proteins and retroviral Gag proteins, which might lead to a different uncoating
477 process for errantiviruses [59]. In our study, we observed the loss of *ZAM* RNA in the oocyte
478 when germline *ZAM*-derived piRNAs are produced. We can hypothesize that the *ZAM* capsid
479 is dissociated soon after entry into the oocyte and that piRNAs can therefore easily target *ZAM*
480 RNAs. It is also possible that *ZAM* RNAs are still encapsidated in the oocyte, but the capsid
481 does not protect the *ZAM* RNA from piRNAs and their associated endonuclease. Previous
482 studies on virus-like particles of the yeast *Ty* retrotransposon suggest that these particles form
483 open structures that leave the RNA at the interior of the capsid accessible to RNase [60,61].
484
485 It has been proposed that in different species, an "innate" response at the piRNA or siRNA level
486 can be initiated in the gonads upon retrovirus invasion ([39,62–67]). We found that no clear innate
487 small RNA response is triggered upon *ZAM* reactivation in Drosophila ovaries. Total small-
488 RNA sequencing after *ZAM* reactivation revealed the presence of sense *ZAM*-mapping small
489 RNAs, but they lack characteristics of siRNAs or piRNAs. We hypothesize that these sense
490 small RNAs are degradation products generated when there is an excessive amount of *ZAM*
491 RNAs. Altogether, these results show that no initial small RNA response is mounted upon *ZAM*
492 reactivation, leaving follicle cells, where *ZAM* is expressed, and also oocytes unprotected
493 against *ZAM* transposition. Our findings suggest that the piRNA response is a robust response
494 that, in the case of *ZAM*, must be established either in the follicle cells or in the germ cells to
495 efficiently control the invading TE. However, the time required for developing a robust piRNA
496 response to sustainably control TE transposition remains unknown. Lastly, it is thought that the
497 piRNA pathway has no antiviral role in Drosophila [68]. However, it would be interesting to
498 determine whether this is also true if parts of the viral genome are integrated into a germline
499 piRNA cluster during infection.

500 Germline and somatic piRNA pathways and their respective piRNA clusters are distinct. There
501 is no ping-pong amplification of piRNAs in the somatic follicle cells and piRNA production in
502 these cells is almost exclusively dependent on a single piRNA cluster, *flamenco*, making it more
503 vulnerable to mutation. A key outcome of our results is that they suggest that not only does the
504 host adapt to the TE but the TE also seems to have adapted to the host: the exclusive expression
505 of *ZAM* in somatic cells allows the TE to "hide" in the follicle cells and invade an unprotected
506 germline after a simple deletion of a short *flam* sequence. The errantivirus *ZAM* thus seems to
507 have adapted to the host by gaining tissue specificity and by adopting an expression niche.
508

509 # Methods

510 **Fly stocks, transgenic lines, and crosses**

511 Flies were maintained at 25°C under a light/dark cycle and 60% humidity. Between 3 and 6
512 days after hatching, flies were used for experiments. The RNAi lines against components of the
513 piRNA pathway used in this study are listed in **Supplementary Table S2**. Isogenic lines from
514 the RevI-H2 stock were generated by crossing a single female with a single male for five
515 generations. Germline and somatic knock-down have been performed using the nanos-gal4 and
516 the traffic-jam-gal4 driver lines respectively (**Supplementary Table S2)**. The Drosophila line
517 carrying the *ZAM* sensor is described in [28]. The sensor expresses the GFP reporter gene under
518 the control of an inducible Upstream Activation Sequence promoter (UASp) and harbors a *ZAM*
519 fragment in its 3′-UTR (pGFP-*ZAM*).
520

521 **Single-molecule RNA fluorescence *in situ* hybridization (smRNA FISH) in ovaries and**
522 **embryos.**

523 *ZAM* smRNA FISH was performed using 48 probes that target *ZAM* transcripts in a region that
524 is absent in the *ZAM* inserted in the *flamenco* piRNA cluster to detect only transcripts of active

525 *ZAM* copies (sequences in Supplementary Table S3). Ovaries from 3 to 6-day-old flies were
526 dissected in Schneider's Drosophila Medium and fixed in Fixing Buffer (4% formaldehyde,
527 0.3% Triton X-100, 1x PBS) for 20 min at room temperature, rinsed three times in 0.3% Triton
528 X-100, once in PBS, and permeabilized in 70% ethanol at 4°C overnight. Permeabilized ovaries
529 were rehydrated in smRNA FISH wash buffer (10% formamide in 2x SSC) for 10 min. Ovaries
530 were resuspended in 50µL hybridization buffer (10% dextran sulfate, 10% formamide in 2x
531 SSC) supplemented with 1µL of smRNA FISH probes. Hybridization was performed with
532 rotation at 37°C overnight. Ovaries were then washed twice with smRNA FISH wash buffer at
533 37°C for 30 min and twice with 2xSSC solution. Then, DNA was stained with DAPI (1/500
534 dilution in 2x SSC) at room temperature for 20 min. Ovaries were mounted in 30 µL
535 Vectashield mounting medium and imaged on a Zeiss LSM-980 or Zeiss LSM-800 confocal
536 microscope. The resulting images were processed using FIJI/ImageJ. The RNA signal
537 specificity was confirmed by adding 1 mg/mL of RNase A in 2x SSC for 2h before the
538 hybridization step.
539 For embryo staining, flies were caged and fed yeast paste. Embryos (0-2h) were collected,
540 dechorionated in 50% bleach for 4 min and rinsed in water. Eggs were fixed in 4%
541 paraformaldehyde/heptane for 20 min, devitellinized by vigorous shaking in 100% methanol
542 and stored in methanol at -20°C. Embryos were rehydrated with 1:1 methanol in 1xPBS, 0.1%
543 Tween-20 for 5 min and twice in 1xPBS, 0.1% Tween-20. Embryos were resuspended in
544 smRNA FISH wash buffer (10% formamide in 2x SSC) for 10 min and then processed for
545 smRNA FISH as described for ovaries. Immunostaining combined with smRNA FISH was
546 performed by adding primary antibodies to the smRNA FISH probes in the hybridization buffer
547 and incubating at 37°C overnight. Embryos were washed twice with smRNA FISH wash buffer
548 and incubated with the secondary antibody for 90 min. After two washes in 2x SSC, embryos
549 were mounted in 30 µL Vectashield mounting medium.

550

551 **Immunofluorescence analysis of ovaries and embryos.**

552 Ovaries from 3-6-day-old flies were dissected in supplemented Schneider's medium, ovarioles
553 were separated, and the muscle sheath was removed before fixation to obtain undistorted
554 follicles. Then, ovaries were fixed in 4% formaldehyde/1x PBS/2% Tween-20 for 15 min,
555 rinsed three times with 1x PBS/2% Tween-20, and incubated 2 hours in PBT (1x PBS, 0.1%
556 Triton X-100, 1% BSA). Ovaries were incubated with primary antibodies in PBT at 4°C
557 overnight (antibodies are described in Supplementary Table S4**)**. After three washes in PBT,
558 ovaries were incubated with the corresponding secondary antibodies coupled to Alexa-488 or
559 Cy3 for 90 min. After two washes in 1x PBS, DNA was stained with DAPI (1/500 dilution in
560 1x PBS) for 20 min. Ovaries were mounted in 30 µL Vectashield mounting medium and imaged
561 on a Zeiss LSM-980 or Zeiss LSM-800 confocal microscope. The resulting images were
562 processed using FIJI/ImageJ.

563

564 **RT-qPCR analysis of transposon expression**

565 10-20 pairs of dissected ovaries were homogenized in TRIzol reagent (Ambion). Following
566 DNase I treatment, cDNA was prepared from 1 µg RNA by random priming of total RNA using
567 Superscript IV Reverse Transcriptase (ThermoFisher Scientific). Quantitative PCR was
568 performed with Roche FastStart SYBR Green Master on a the Lightcycler® 480 Instrument.
569 RT-qPCR was used for quantification of transposon mRNA levels (primer sequences in
570 Supplementary Table S5). All experiments were done with three biological replicates and with
571 technical triplicates. Steady-state RNA levels were calculated from the threshold cycle for
572 amplification with the $2^{-\Delta\Delta CT}$ method; *rp49* was used for normalization.

573

574 **Immunoprecipitation of Piwi-ribonucleoprotein complexes**

575 For each genotype, 50 pairs of ovaries from 3-6-day-old flies were dissected, lysed in 1 ml lysis
576 buffer (20 mM HEPES-NaOH at pH 7.0, 150 mM NaCl, 2.5 mM $MgCl_2$, 250 mM sucrose,
577 0.05% NP40, 0.5% Triton X-100, 1x Roche-Complete). Samples were cleared by centrifugation
578 at 10000 × g at 4°C for 10 min. Extracts were incubated with rotation with rabbit polyclonal
579 anti-Piwi antibodies (4 µg per sample) at 4°C for 4h followed by overnight incubation with
580 Dynabeads™ Protein A (50 µl, Invitrogen, 10002D) at 4°C with rotation. Before incubation,
581 beads were equilibrated in NT2 buffer (50 mM Tris-HCl, pH 7.4, 150 mM NaCl, 1 mM $MgCl_2$,
582 0.05% NP40). Beads were washed twice with ice-cold NT2 and twice with NT2 in which NaCl
583 concentration was adjusted to 300 mM. Nucleic acids that co-immunoprecipitated with Piwi
584 were isolated by treating beads with 0.7 mg/ml proteinase K in 0.3ml proteinase K buffer (0.5%
585 SDS, 10mM Tris-HCl pH 7.4, 50mM NaCl, 5mM EDTA), followed by phenol/chloroform
586 extraction (phenol at neutral pH) and ethanol precipitation.
587
588 **DNA Isolation, Oxford Nanopore Technology sequencing and genome analysis**
589 DNA was extracted from 200 RevI-H2i2 females using the Qiagen Blood & Cell Culture DNA
590 Midi kit. The genomic DNA quality and quantity were evaluated using a Femto Pulse (Agilent)
591 and a Qbit 3.0 (Invitrogen) respectively. Oxford Nanopore Technology (ONT) sequencing was
592 performed by I2BC (Gif-sur-Yvette, France) using five micrograms of genomic DNA. Adapter-
593 trimmed ONT reads were analyzed using NCBI Blastn
594 (https://blast.ncbi.nlm.nih.gov/Blast.cgi) or command-line Blastn (Blastn 2.8.1). The RevI-
595 H2i2 ONT reads containing *ZAM* insertions were detected by Blastn with the reference *ZAM*
596 [22], Repbase *ZAM*_I and *ZAM*_LTR sequences (https://www.girinst.org/repbase/, [29]). The *ZAM*
597 containing reads were then recovered with bedtools getfasta
598 (https://bedtools.readthedocs.io/en/latest/content/tools/getfasta.html, [69]). The *ZAM* insertion
599 sites where determined using Blastn of the *ZAM* containing reads to the *D. melanogaster*

600 Release 6 genome (http://flybase.org). The absence of empty sites, without a given *ZAM*
601 insertion, was verified by Blastn of the respective empty insertion sites, recovered from the *D.*
602 *melanogaster* Release 6 genome, to all ONT reads. Sequencing data are available in NCBI GEO
603 database (GSE213456).
604
605 RNA-sequencing and analysis
606 3 independent total RNA extractions from 30 ovaries from 3-6-day-old RevI-H2i2 flies using
607 Trizol (Invitrogen) were performed. Strand-specific libraries for RNA sequencing (RNA-Seq)
608 were constructed at BGI. 1 µg of total RNA was used to prepare mRNA library using MGIEasy
609 RNA Library Prep kit and sequenced as PE150 reads on the DNBSEQ G400 sequencer, and
610 adapter-clipped reads were provided by BGI. The data were analyzed on the local Galaxy
611 platform using HISAT2 alignment (Galaxy Version 2.1.0). The reads were first mapped to
612 *ZAM-fl* and to *ZAM-v2* using the "Disable spliced alignment" option. The mapped reads were
613 then aligned to ZAM_I sequence (Repbase) with the default options, i.e. allowing split
614 alignment. Reads were visualized using "Integrative Genomics Viewer" version 2.16.1. The
615 coverage of RNA-seq reads corresponding to *ZAM-v2* was determined as the number of split
616 reads specific to the *ZAM-v2* deletion at positions ZAM_I:5494-6120, normalized to the
617 average coverage of the pointed transcript. Coverage of RNA-seq reads corresponding to ZAM-
618 fl and ZAM-v2 was determined as the number of non-split reads at position 5495, the left edge
619 of the deletion, normalized to the average coverage of the pointed transcript. Only the left edge
620 was used for this purpose, as the right edge of the deletion is also mapped by reads
621 corresponding to ZAM-variants with other internal deletions (green in Figure 1a).
622
623 **Small RNA sequencing**

624 Regulatory small RNA extraction was performed as described in [70]. Briefly, 50 pairs of ovaries
625 from 3-6-day-old flies were lysed and Argonaute-small RNA complexes were isolated using
626 TraPR ion exchange spin columns (Lexogen, Catalog Nr.128.08). Total RNA also was
627 extracted for some samples (80-100 ovaries for each sample) using the classical TRIzol
628 extraction, followed by 2S rRNA depletion and size selection before sequencing. Sequencing
629 was performed by Fasteris SA (Geneva, Switzerland) on an Illumina NextSeq550 instrument
630 (13-15 million reads per sample).
631 Illumina small RNA sequencing reads were loaded on the small RNA analysis pipeline
632 sRNAPipe [71] for mapping to the various genomic sequence categories of the *D. melanogaster*
633 genome (Release 6). For the analysis, 23-29nt genome mappers were selected as piRNAs, and
634 21nt genome mappers were selected as siRNAs. "Genome-unique" piRNAs were defined as
635 23-29 reads that mapped uniquely across the reference genome. piRNAs were mapped to TEs
636 allowing up to 3 mismatches, siRNAs allowing up to 1 mismatch, and genome-unique piRNAs
637 to piRNA clusters as defined in [11] allowing no mismatch. The window size was of 91nt for the
638 entire *ZAM*, 86 nt for ZAM_I and 140nt for the *flamenco* region at X:21,769,891..21,789,891
639 to establish the piRNA density profiles. For comparison between samples, all read counts were
640 normalized by the number of piRNA/siRNA reads used as input (genome-mapped piRNAs or
641 siRNAs, genome-unique piRNAs) and represented in RPM [RPM = read-count * 1,000,000 /
642 (total of genome mapping piRNAs)], or RPKM [RPM = read-count * 1,000,000 / (TE
643 Length/1000) / (total of genome mapping piRNAs)] in the case of density profiles. To assess
644 the ping-pong signature, the counts of 1 to 23nt 5'-overlaps were determined, and the percentage
645 of 10nt 5'-overlaps over the total 1-23nt 5'-overlaps was calculated. The Z-score for 10nt
646 5’overlaps was determined using the percentages of all 1 to 23nt-long 5’overlaps as a
647 background and was considered significant when it was >1.96. Scatter plots were done with
648 RStudio with antisense piRNAs or siRNAs mapping to the respective internal sequence of TEs

649 (allowing 0-3 mismatches for piRNAs and 0-1 mismatch for siRNAs). All small RNA
650 sequencing done for this study is listed in Supplementary Table S6**.** Small-RNA sequencing
651 data are available in NCBI GEO database (GSE213368).
652
653 **Sterility tests**
654 For the sterility tests, RevI-H2i2 homozygous females were compared to w^{1118} females, and
655 homozygous *flamΔZAM* females that carry three functional *ZAM* copies from the RevI-H2 X
656 chromosome were compared to *flamΔZAM* females without these functional *ZAM* copies in
657 their genome. Sterility tests were performed at 25° C. Thirty 3-6-day-old virgin females of each
658 genotype were individually mated with three w^{1118} males, and eggs were collected for 24 hours.
659 The number of eggs laid by each female was determined. Then, eggs were kept at 25°C for
660 another 24 hours before determining the egg hatching rate. The experiment was done twice for
661 a total of approximatively 60 replicates for each condition.
662
663 **Generation of the *flamΔZAM* line using the CRISPR-Cas9 technology**
664 The *ZAM* copy in the *flamenco* piRNA cluster was deleted using a pCFD6 plasmid that
665 expresses two single guide RNAs (sgRNAs) under the Gal4/UAS system. The sgRNAs were
666 designed to target genome-unique sequences located upstream and downstream of the *flamenco*
667 *ZAM* copy: TTGTAGCGCTCTTCTTCTCT (sgRNA *flamΔZAM_1*) and
668 AGCGCAACCACGTACAGCGA (sgRNA *flamΔZAM_2*). The pCFD6 plasmid harboring
669 these sgRNAs was injected by the Bestgene company into embryos from the BL#9736 stock
670 (Bloomington stock center) for integration of the plasmid into the genomic site 53B2. The
671 obtained flies were crossed with nanos-gal4; UAS-Cas9 flies (BL#54593, Bloomington stock
672 center). Prior to crossing, the X chromosome of each of these lines was replaced by the X
673 chromosome of the Iso1A *Drosophila* line. After the crosses, 500 lines were derived and

674 screened by PCR using primers specific for the *flamenco ZAM* copy. The detailed crossing
675 schemes are available upon request. Lines without amplification of internal *flamenco ZAM*
676 sequences were selected for PCR amplification of the target locus with primers that framed the
677 *flamenco ZAM* copy and the target sequences of the sgRNAs. The obtained amplicons were
678 sequenced.
679

680 ACKNOWLEDGEMENTS

681 We thank the *Bloomington Stock Center* for providing stocks. We thank J. Brennecke for
682 providing antibodies. We thank www.flybase.org, "http://www.girinst.org"and NCBI for
683 providing databases and tools. We thank S. Chambeyron and K. Senti for helpful discussions,
684 A. Molaro and the members of the Brasset laboratory for comments on the manuscript. We
685 thank C. Vaury for having established the original RevI-H2 line over 30 years ago, and for
686 preserving it all these years. We thank Y. Renaud and P. Pouchin for helpful advices and
687 development of the iGReD bioinfomatics platform. We also thank the CLIC facility (Clermont
688 Imagerie Confocale). We thank Gentyane Facility for the Quality Control of gDNA.
689

690 AUTHOR CONTRIBUTIONS

691 Conceptualization, MY, SJ and EB; Validation and Investigation, MY, SMM, AA, NG, BB,
692 Data curation and bioinformatic analyses, MY, SJ, writing—original draft, MY and EB;
693 writing—review and editing, MY, SJ and EB; Supervision, SJ and EB, funding acquisition,
694 MY and EB.
695

696 FUNDING

697

698 This work was supported by grants from the Agence Nationale pour la Recherche (CHApiTRE

ANR-20-CE12-0005, BiopiC ANR-21-CE12-0022, and EpiTET ANR-17-CE12-0030-03), the La Fondation ARC pour la recherche sur le cancer (PJA20171206129). M.Y. was supported by the Ministère de l'Enseignement Supérieur et de la Recherche and the Fondation pour la Recherche Médicale (FDT202106012950). This research was financed by the French government IDEX-ISITE initiative 16-IDEX-0001 (CAP 20-25). The funders had no role in study design, data collection and analysis, decision to publish, or preparation of the manuscript.

COMPETING INTERESTS

The authors declare that no competing interest exists**.**

REFERENCES

1. Dewannieux, M. *et al.* The mouse IAPE endogenous retrovirus can infect cells through any of the five GPI-anchored Ephrin A proteins. *PLoS Pathog.* **7**, e1002309 (2011).
2. Frank, J. A. *et al.* Evolution and antiviral activity of a human protein of retroviral origin. *Science* **378**, 422–428 (2022).
3. Grow, E. J. *et al.* Intrinsic retroviral reactivation in human preimplantation embryos and pluripotent cells. *Nature* **522**, 221–225 (2015).
4. Svoboda, P. *et al.* RNAi and expression of retrotransposons MuERV-L and IAP in preimplantation mouse embryos. *Dev. Biol.* **269**, 276–285 (2004).
5. Tokuyama, M. *et al.* ERVmap analysis reveals genome-wide transcription of human endogenous retroviruses. *Proc. Natl. Acad. Sci. U. S. A.* **115**, 12565–12572 (2018).
6. Gerdes, P., Richardson, S. R., Mager, D. L. & Faulkner, G. J. Transposable elements in the mammalian embryo: pioneers surviving through stealth and service. *Genome Biol.* **17**, 100 (2016).

726 7. Nicolau, M., Picault, N. & Moissiard, G. The Evolutionary Volte-Face of Transposable
727 Elements: From Harmful Jumping Genes to Major Drivers of Genetic Innovation. *Cells*
728 **10**, (2021).
729 8. Ozata, D. M., Gainetdinov, I., Zoch, A., O'Carroll, D. & Zamore, P. D. PIWI-interacting
730 RNAs: small RNAs with big functions. *Nat. Rev. Genet.* **20**, 89–108 (2019).
731 9. Czech, B. *et al.* piRNA-Guided Genome Defense: From Biogenesis to Silencing. *Annu.*
732 *Rev. Genet.* **52**, 131–157 (2018).
733 10. King, R. C., Aggarwal, S. K. & Aggarwal, U. The development of the female Drosophila
734 reproductive system. *J. Morphol.* **124**, 143–166 (1968).
735 11. Brennecke, J. *et al.* Discrete small RNA-generating loci as master regulators of
736 transposon activity in Drosophila. *Cell* **128**, 1089–1103 (2007).
737 12. Pélisson, A. *et al.* Gypsy transposition correlates with the production of a retroviral
738 envelope-like protein under the tissue-specific control of the Drosophila flamenco gene.
739 *EMBO J.* **13**, 4401–4411 (1994).
740 13. Desset, S., Meignin, C., Dastugue, B. & Vaury, C. COM, a heterochromatic locus
741 governing the control of independent endogenous retroviruses from Drosophila
742 melanogaster. *Genetics* **164**, 501–509 (2003).
743 14. Zanni, V. *et al.* Distribution, evolution, and diversity of retrotransposons at the
744 flamenco locus reflect the regulatory properties of piRNA clusters. *Proc. Natl. Acad. Sci.*
745 *U. S. A.* **110**, 19842–19847 (2013).
746 15. Desset, S., Buchon, N., Meignin, C., Coiffet, M. & Vaury, C. In Drosophila melanogaster
747 the COM locus directs the somatic silencing of two retrotransposons through both Piwi-
748 dependent and -independent pathways. *PLoS One* **3**, (2008).

749 16. Lau, N. C. *et al.* Abundant primary piRNAs, endo-siRNAs, and microRNAs in a Drosophila
750 ovary cell line. *Genome Res.* **19**, 1776–1785 (2009).
751 17. Leblanc, P. *et al.* Life Cycle of an Endogenous Retrovirus, ZAM, in Drosophila
752 melanogaster. *J. Virol.* **74**, 10658–10669 (2000).
753 18. Song, S. U., Kurkulos, M., Boeke, J. D. & Corces, V. G. Infection of the germ line by
754 retroviral particles produced in the follicle cells: A possible mechanism for the
755 mobilization of the gypsy retroelement of Drosophila. *Development* **124**, 2789–2798
756 (1997).
757 19. Keegan, R. M., Talbot, L. R., Chang, Y. H., Metzger, M. J. & Dubnau, J. Intercellular viral
758 spread and intracellular transposition of Drosophila gypsy. *PLoS Genet.* **17**, 1–22 (2021).
759 20. Brasset, E. *et al.* Viral particles of the endogenous retrovirus ZAM from Drosophila
760 melanogaster use a pre-existing endosome/exosome pathway for transfer to the
761 oocyte. *Retrovirology* **3**, 1–9 (2006).
762 21. Tcheressiz, S. *et al.* Expression of the Idefix retrotransposon in early follicle cells in the
763 germarium of Drosophila melanogaster is determined by its LTR sequences and a
764 specific genomic context. *Mol. Genet. Genomics* **267**, 133–141 (2002).
765 22. Sokolova, O. A. *et al.* Special vulnerability of somatic niche cells to transposable
766 element activation in Drosophila larval ovaries. *Sci. Rep.* **10**, (2020).
767 23. Malone, C. D. *et al.* Specialized piRNA Pathways Act in Germline and Somatic Tissues of
768 the Drosophila Ovary. *Cell* **137**, 522–535 (2009).
769 24. Chalvet, F. *et al.* Proviral amplification of the Gypsy endogenous retrovirus of
770 Drosophila melanogaster involves env-independent invasion of the female germline.
771 *EMBO J.* **18**, 2659–2669 (1999).

772 25. Bline, A. P., Le Goff, A. & Allard, P. What Is Lost in the Weismann Barrier? *Journal of*
773 *developmental biology* **8**, (2020).
774 26. Leblanc, P., Desset, S., Dastugue, B. & Vaury, C. Invertebrate retroviruses: ZAM a new
775 candidate in D. melanogaster. *EMBO J.* **16**, 7521–7531 (1997).
776 27. Desset, S. *et al.* Mobilization of two retroelements, ZAM and Idefix, in a novel unstable
777 line of Drosophila melanogaster. *Mol. Biol. Evol.* **16**, 54–66 (1999).
778 28. Duc, C. *et al.* Trapping a somatic endogenous retrovirus into a germline piRNA cluster
779 immunizes the germline against further invasion. *Genome Biol.* **20**, 1–14 (2019).
780 29. Jurka, J. *et al.* Repbase Update, a database of eukaryotic repetitive elements.
781 *Cytogenet. Genome Res.* **110**, 462–467 (2005).
782 30. George, P. *et al.* Increased production of piRNAs from euchromatic clusters and genes
783 in Anopheles gambiae compared with Drosophila melanogaster. *Epigenetics and*
784 *Chromatin* **8**, (2015).
785 31. Czech, B. & Hannon, G. J. One Loop to Rule Them All: The Ping-Pong Cycle and piRNA-
786 Guided Silencing. *Trends Biochem. Sci.* **41**, 324–337 (2016).
787 32. Meignin, C., Dastugue, B. & Vaury, C. Intercellular communication between germ line
788 and somatic line is utilized to control the transcription of ZAM, an endogenous
789 retrovirus from Drosophila melanogaster. *Nucleic Acids Res.* **32**, 3799–3806 (2004).
790 33. Atallah, J. & Lott, S. E. Evolution of maternal and zygotic mRNA complements in the
791 early Drosophila embryo. *PLoS Genet.* **14**, e1007838 (2018).
792 34. Aravin, A. A. & Hannon, G. J. Small RNA silencing pathways in germ and stem cells. *Cold*
793 *Spring Harb. Symp. Quant. Biol.* **73**, 283–290 (2008).
794 35. Khurana, J. S. & Theurkauf, W. piRNAs, transposon silencing, and Drosophila germline
795 development. *J. Cell Biol.* **191**, 905–913 (2010).

796 36. Saito, K. & Siomi, M. C. Small RNA-mediated quiescence of transposable elements in
797 animals. *Dev. Cell* **19**, 687–697 (2010).
798 37. Klattenhoff, C. *et al.* Drosophila rasiRNA pathway mutations disrupt embryonic axis
799 specification through activation of an ATR/Chk2 DNA damage response. *Dev. Cell* **12**,
800 45–55 (2007).
801 38. Parameswaran, P. *et al.* Six RNA viruses and forty-one hosts: viral small RNAs and
802 modulation of small RNA repertoires in vertebrate and invertebrate systems. *PLoS*
803 *Pathog.* **6**, e1000764 (2010).
804 39. Yu, T. *et al.* The piRNA Response to Retroviral Invasion of the Koala Genome. *Cell* **179**,
805 632-643.e12 (2019).
806 40. Le Rouzic, A. & Capy, P. The first steps of transposable elements invasion: Parasitic
807 strategy vs. genetic drift. *Genetics* **169**, 1033–1043 (2005).
808 41. Kofler, R., Senti, K. A., Nolte, V., Tobler, R. & Schlötterer, C. Molecular dissection of a
809 natural transposable element invasion. *Genome Res.* **28**, 824–835 (2018).
810 42. Robillard, É., Le Rouzic, A., Zhang, Z., Capy, P. & Hua-Van, A. Experimental evolution
811 reveals hyperparasitic interactions among transposable elements. *Proc. Natl. Acad. Sci.*
812 *U. S. A.* **113**, 14763–14768 (2016).
813 43. Schaack, S., Gilbert, C. & Feschotte, C. Promiscuous DNA: Horizontal transfer of
814 transposable elements and why it matters for eukaryotic evolution. *Trends Ecol. Evol.*
815 **25**, 537–546 (2010).
816 44. Wierzbicki, F., Kofler, R. & Signor, S. Evolutionary dynamics of piRNA clusters in
817 Drosophila. *Mol. Ecol.* 1–17 (2021).

818 45. Yoth, M., Jensen, S. & Brasset, E. The Intricate Evolutionary Balance between
819 Transposable Elements and Their Host: Who Will Kick at Goal and Convert the Next Try?
820 *Biology* **11**, (2022).
821 46. Mohn, F., Sienski, G., Handler, D. & Brennecke, J. The Rhino-Deadlock-Cutoff complex
822 licenses noncanonical transcription of dual-strand piRNA clusters in Drosophila. *Cell*
823 **157**, 1364–1379 (2014).
824 47. Luo, S. *et al.* The evolutionary arms race between transposable elements and piRNAs in
825 Drosophila melanogaster. *BMC Evol. Biol.* **20**, 1–18 (2020).
826 48. Gebert, D. *et al.* Large Drosophila germline piRNA clusters are evolutionarily labile and
827 dispensable for transposon regulation. *Mol. Cell* 1–14 (2021).
828 49. Shpiz, S., Ryazansky, S., Olovnikov, I., Abramov, Y. & Kalmykova, A. Euchromatic
829 Transposon Insertions Trigger Production of Novel Pi- and Endo-siRNAs at the Target
830 Sites in the Drosophila Germline. *PLoS Genet.* **10**, (2014).
831 50. Kofler, R. Dynamics of transposable element invasions with piRNA clusters. *Mol. Biol.*
832 *Evol.* **36**, 1457–1472 (2019).
833 51. Lerat, E. *et al.* Population-specific dynamics and selection patterns of transposable
834 element insertions in European natural populations. *Mol. Ecol.* **28**, 1506–1522 (2019).
835 52. Feschotte, C. & Wessler, S. R. Mariner-like transposases are widespread and diverse in
836 flowering plants. *Proc. Natl. Acad. Sci. U. S. A.* **99**, 280–285 (2002).
837 53. Navarro-Costa, P. *et al.* Early programming of the oocyte epigenome temporally
838 controls late prophase i transcription and chromatin remodelling. *Nat. Commun.* **7**,
839 (2016).
840 54. Bergeron, F., Leduc, R. & Day, R. Subtilase-like pro-protein convertases: from molecular
841 specificity to therapeutic applications. *J. Mol. Endocrinol.* **24**, 1–22 (2000).

842 55. Klenk, H. D. & Garten, W. Host cell proteases controlling virus pathogenicity. *Trends*
843 *Microbiol.* **2**, 39–43 (1994).
844 56. Malik, H. S., Henikoff, S. & Eickbush, T. H. Poised for contagion: evolutionary origins of
845 the infectious abilities of invertebrate retroviruses. *Genome Res.* **10**, 1307–1318 (2000).
846 57. Hosaka, M. *et al.* Arg-X-Lys/Arg-Arg motif as a signal for precursor cleavage catalyzed by
847 furin within the constitutive secretory pathway. *J. Biol. Chem.* **266**, 12127–12130
848 (1991).
849 58. Guedán, A., Caroe, E. R., Barr, G. C. R. & Bishop, K. N. The Role of Capsid in HIV-1
850 Nuclear Entry. *Viruses* **13**, (2021).
851 59. Syomin, B. V., Kandror, K. V., Semakin, A. B., Tsuprun, V. L. & Stepanov, A. S. Presence of
852 the gypsy (MDG4) retrotransposon in extracellular virus-like particles. *FEBS Lett.* **323**,
853 285–288 (1993).
854 60. Palmer, K. J. *et al.* Cryo-electron microscopy structure of yeast Ty retrotransposon virus-
855 like particles. *J. Virol.* **71**, 6863–6868 (1997).
856 61. Burns, N. R. *et al.* Symmetry, flexibility and permeability in the structure of yeast
857 retrotransposon virus-like particles. *EMBO J.* **11**, 1155–1164 (1992).
858 62. Kolliopoulou, A. *et al.* PIWI pathway against viruses in insects. *Wiley Interdiscip. Rev.*
859 *RNA* **10**, e1555 (2019).
860 63. Rozhkov, N. V. *et al.* Small RNA-based silencing strategies for transposons in the process
861 of invading Drosophila species. *RNA* **16**, 1634–1645 (2010).
862 64. Rozhkov, N. V. *et al.* Evolution and dynamics of small RNA response to a retroelement
863 invasion in drosophila. *Mol. Biol. Evol.* **30**, 397–408 (2013).
864 65. Kawamura, Y. *et al.* Drosophila endogenous small RNAs bind to Argonaute 2 in somatic
865 cells. *Nature* **453**, 793–797 (2008).

866 66. Rehwinkel, J. *et al.* Genome-Wide Analysis of mRNAs Regulated by Drosha and
867 Argonaute Proteins in Drosophila melanogaster. *Mol. Cell. Biol.* **26**, 2965–2975 (2006).
868 67. Katsuma, S. *et al.* Transcriptome profiling reveals infection strategy of an insect
869 maculavirus. *DNA Res.* **25**, 277–286 (2018).
870 68. Petit, M. *et al.* piRNA pathway is not required for antiviral defense in Drosophila
871 melanogaster. *Proceedings of the National Academy of Sciences* **113**, E4218–E4227
872 (2016).
873 69. Quinlan, A. R. & Hall, I. M. BEDTools: a flexible suite of utilities for comparing genomic
874 features. *Bioinformatics* **26**, 841–842 (2010).
875 70. Grentzinger, T. *et al.* A universal method for the rapid isolation of all known classes of
876 functional silencing small RNAs. *Nucleic Acids Res.* **48**, (2020).
877 71. Pogorelcnik, R., Vaury, C., Pouchin, P., Jensen, S. & Brasset, E. sRNAPipe: A Galaxy-based
878 pipeline for bioinformatic in-depth exploration of small RNAseq data. *Mob. DNA* **9**, 4–9
879 (2018).
880
881
882
883
884
885
886
887
888

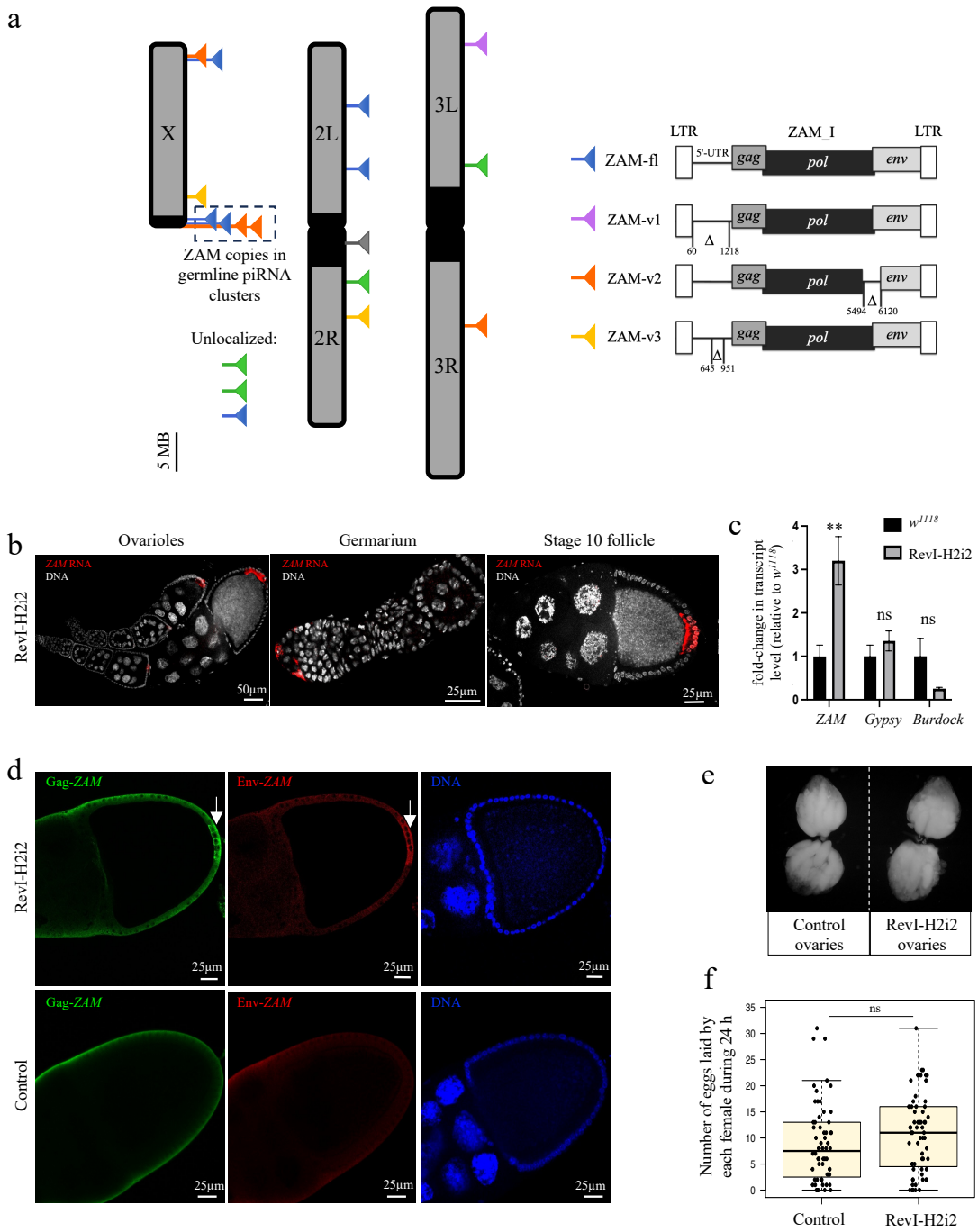

Figure 1: *ZAM* is expressed in follicle cells in the RevI-H2i2 isogenic line but the line is stable.

a. *ZAM* elements in the RevI-H2i2 genome. Each triangle represents a *ZAM* insertion. The different ZAM-variants are presented in the illustration on the right. The positions refer to *ZAM* internal sequences (*ZAM*_I in RepBase). Blue: full-length *ZAM* elements (ZAM-fl); violet: *ZAM* variants *ZAM-v1* with deleted 5'-UTR; orange: *ZAM*-variants *ZAM-v2*, in which positions 5494-6120 are deleted; yellow: ZAM-variants ZAM-v3 with a 303 bp deletion in the 5'-UTR; green: *ZAM* with internal deletions other than *ZAM* variants above; gray: full-length *ZAM* copy also present in the reference Release 6 genome (http://flybase.org). The dotted box indicates four *ZAM* copies on the X chromosome inserted in referenced germline piRNA clusters (Cluster

9 and 13). No *ZAM* insertion was found in chromosome 4 (1.35 Mb, not shown). For coordinates and details see Supplementary Table 1. **b**. Projection of confocal images of ovarioles, germarium, and stage 10 follicles showing *ZAM* expression by smRNA FISH (in red) in RevI-H2i2 ovaries. DNA was stained with DAPI (white). **c**. Fold-change in the steady-state *ZAM*, *Gypsy* and *Burdock* RNA levels for RevI-H2i2 ovaries compared with w^{1118} ovaries (control), quantified by RT-qPCR (primer sequences in Supplementary Table 5). At least three biological replicates and three technical replicates were used. ***p-value* <0.01; ns, not-significant (*p-value* >0.05) (Mann-Whitney test). Error bars indicate the standard deviation (SD). **d**. Confocal sections of stage 10 egg chambers of RevI-H2i2 and w^{1118} control line showing *ZAM*-encoded Gag (green) and Env (red) proteins. DNA was stained with DAPI (white). **e**. Morphology of control and RevI-H2i2 ovaries. **f.** Box plot displaying the number of eggs laid per fly per day by control and RevI-H2i2 females. Each dot represents an individual female. The midline indicates the median value, and the box shows the first and third quartile. Error bars indicate the SD. ns, not-significant (*p-value* >0.05) (Mann-Whitney test).

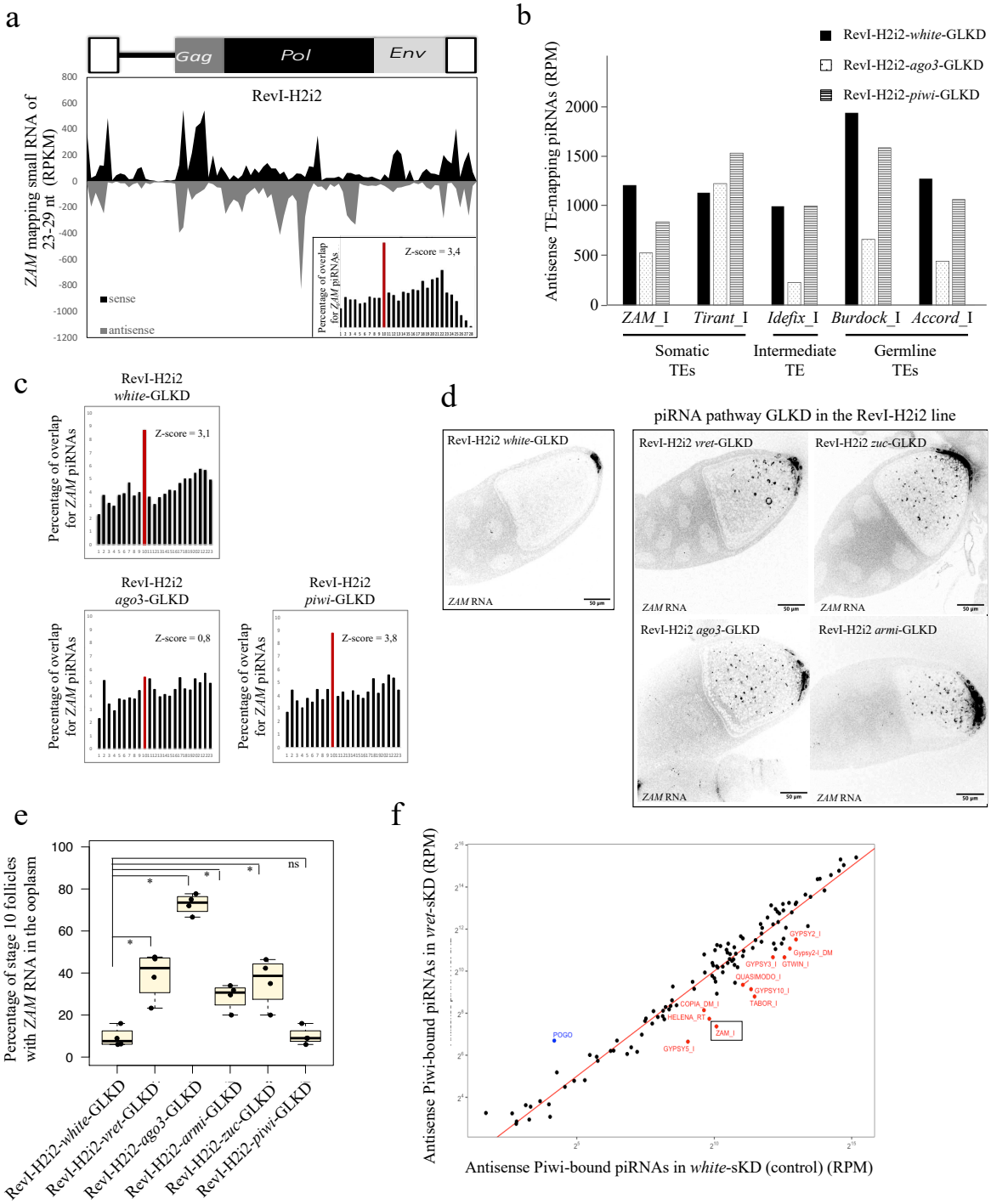
a
Gag
Pol
Env
RevI-H2i2
ZAM mapping small RNA of 23-29 nt (RPKM)
sense
antisense
Z-score = 3,4
Percentage of overlap for ZAM piRNAs
b
RevI-H2i2-white-GLKD
RevI-H2i2-ago3-GLKD
RevI-H2i2-piwi-GLKD
Antisense TE-mapping piRNAs (RPM)
ZAM_I
Tirant_I
Idefix_I
Burdock_I
Accord_I
Somatic TEs
Intermediate TE
Germline TEs
c
RevI-H2i2 white-GLKD
Z-score = 3,1
RevI-H2i2 ago3-GLKD
Z-score = 0,8
RevI-H2i2 piwi-GLKD
Z-score = 3,8
d
piRNA pathway GLKD in the RevI-H2i2 line
RevI-H2i2 white-GLKD
RevI-H2i2 vret-GLKD
RevI-H2i2 zuc-GLKD
RevI-H2i2 ago3-GLKD
RevI-H2i2 armi-GLKD
ZAM RNA
e
Percentage of stage 10 follicles with ZAM RNA in the ooplasm
ns
RevI-H2i2-white-GLKD
RevI-H2i2-vret-GLKD
RevI-H2i2-ago3-GLKD
RevI-H2i2-armi-GLKD
RevI-H2i2-zuc-GLKD
RevI-H2i2-piwi-GLKD
f
Antisense Piwi-bound piRNAs in vret-sKD (RPM)
Antisense Piwi-bound piRNAs in white-sKD (control) (RPM)
POGO
GYPSY5_I
HELENA_RT
COPIA_DM_I
ZAM_I
TABOR_I
GYPSY10_I
QUASIMODO_I
GYPSY3_I
GTWIN_I
Gypsy2-I_DM
GYPSY2_I
g
white-sKD
vret-sKD
ZAM RNA
DNA
50µm
h
vret-sKD – stage 10 follicle
ZAM RNA
25µm
i
Percentage of stage 10 follicles with ZAM RNA invasion in the ooplasm
white-sKD
vret-sKD

917
918

Figure 2: Germline *ZAM* piRNAs produced in RevI-H2i2 germ cells counteract *ZAM* invasion.

a. Density plot of *ZAM*-mapping regulatory piRNAs along the *ZAM* sequence in RevI-H2i2 ovaries (up to 3 mismatches). In the lower right corner is the histogram showing the percentage of 5'-overlaps between sense and antisense *ZAM*-derived piRNAs (23–29 nt) in RevI-H2i2 ovaries. The proportion of 10nt 5'-overlaps is in red and the corresponding Z-score is indicated. **b.** Antisense piRNAs mapping to TE internal sequences (0-3 mismatches) in the RevI-H2i2 line upon *white*- (control), *ago3-,* or *piwi*-GLKD. Normalized per million of genome-mapping piRNAs. **c.** Histogram showing the percentage of 5'-overlaps between sense and antisense *ZAM*-mapping piRNAs (up to 3 mismatches) in *white-, ago3-,* or *piwi*-GLKD RevI-H2i2 ovaries. The percentage of 10nt overlaps is in red and the corresponding Z-score is indicated. **d.** Color-inverted confocal images of stage 10 egg chambers showing *ZAM* smRNA FISH signal in ovaries of the indicated genotypes. **e.** Bar plot showing the percentage of stage 10 follicles with *ZAM* RNA detected in the ooplasm by smRNA FISH of RevI-H2i2 ovaries with the indicated GLKD. This experiment was done three times and approximately 50 follicles per conditions were observed for each experiment. Error bars indicate the SD. **f.** Scatter plot showing the normalized counts of antisense Piwi-bound piRNAs mapping to individual internal TEs sequences in control ovaries (*white*-sKD) and *vret*-sKD ovaries. Antisense piRNA counts, mapped allowing up to 3 mismatches, were normalized per million of genome-mapping piRNAs (RPM, here in logarithmic scale). TEs in red have a *vret*-sKD/*white*-sKD ratio <0.3. *ZAM* is boxed black. **g.** Confocal images of ovarioles showing *ZAM* smRNA FISH signal (in red) in *white*- (control) and v*ret*-sKD ovaries. DNA was stained with DAPI (white). **h**. Color-inverted confocal projection of stage 10 egg chamber showing *ZAM sm*RNA FISH signal in *vret*-sKD ovaries. **i.** Bar plot showing the percentage of stage 10 follicles with *ZAM* RNA invasion of the ooplasm, assessed by *ZAM* smRNA FISH, of *white*- (control) and *vret*-sKD ovaries. This experiment was done twice and ~50 follicles per condition were observed for each experiment. Error bars indicate the SD.

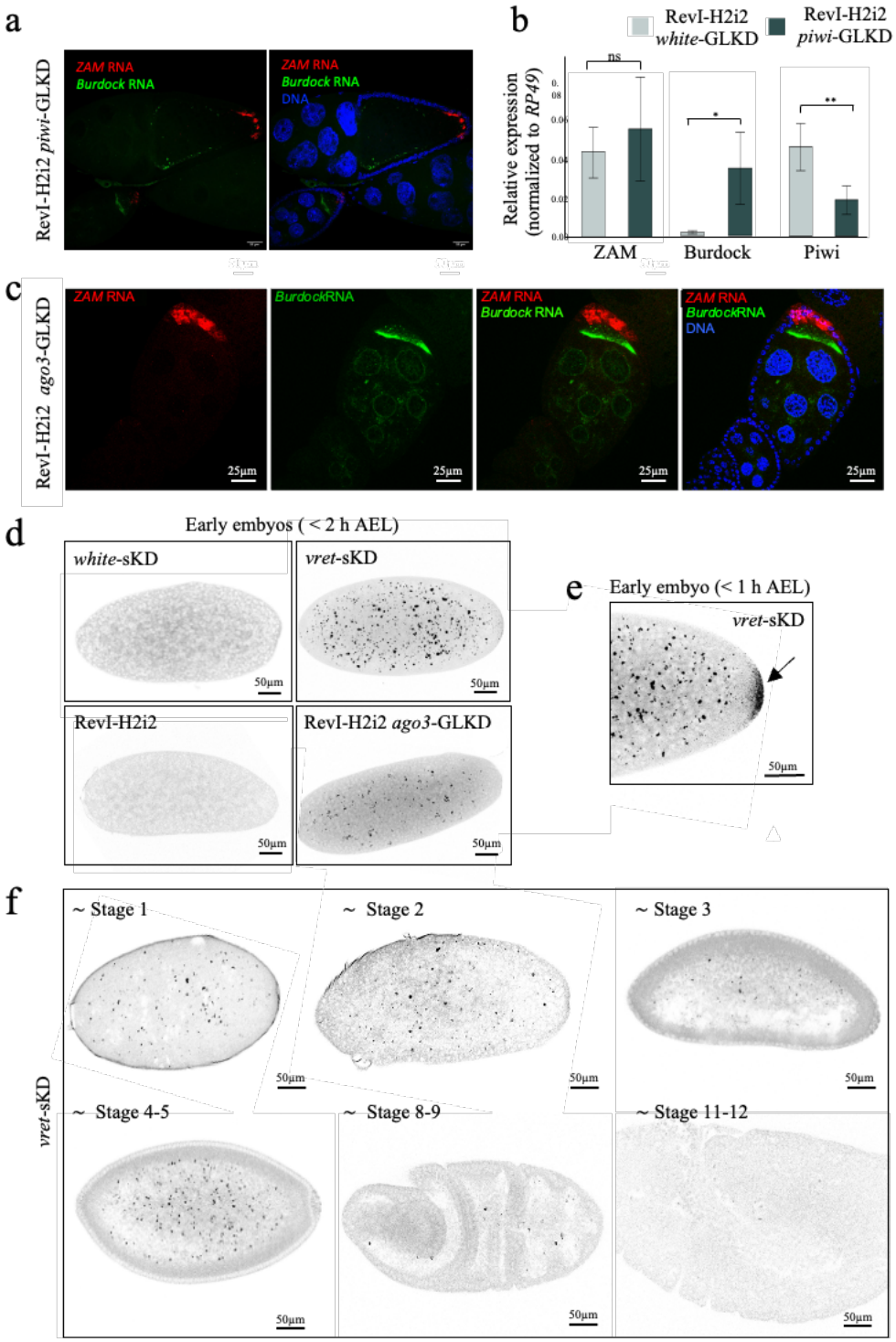

Figure 3: *ZAM* RNAs transcribed in the follicle cells transit to the oocyte and are deposited in early embryos.

a. Confocal images of stage 10 follicles in the RevI-H2i2 *piwi*-GLKD line. *Burdock* (green) and *ZAM* (red) mRNAs were detected by smRNA FISH. DNA was stained with DAPI (blue). **b**. Fold-change in the steady-state *ZAM*, *Burdock* and *Piwi* RNA levels for RevI-H2i2 *piwi*-GLKD ovaries compared with RevI-H2i2 *white*-GLKD ovaries (control), quantified by RT-qPCR (primer sequences in Supplementary Table 5). At least three biological replicates and three technical replicates were used. *: *p*-value < 0.05, **: p-*value* <0.01; ns, not significant (*p-value* >0.05) (Mann-Whitney test). Error bars indicate the standard deviation (SD) **c.** Confocal

960 images of ovarioles and of an isolate stage 8 egg chamber in the RevI-H2i2 *ago3*-GLKD line.
961 *Burdock* (green) and *ZAM* (red) mRNAs were detected by smRNA FISH. DNA was stained
962 with DAPI (blue). **d.** Color-inverted confocal images showing *ZAM* smRNA FISH signal in
963 early embryos collected 0-2 hours after egg laying (AEL). Mothers were from the indicated
964 genotype. **e.** Zoom on the posterior part of a *vret*-sKD early embryo collected at 0-1 hours AEL
965 showing *ZAM* RNA accumulation at the posterior pole. **f.** Color-inverted confocal images
966 showing *ZAM* smRNA FISH signal in embryos laid by *vret*-sKD females at the indicated
967 developmental stages.
968

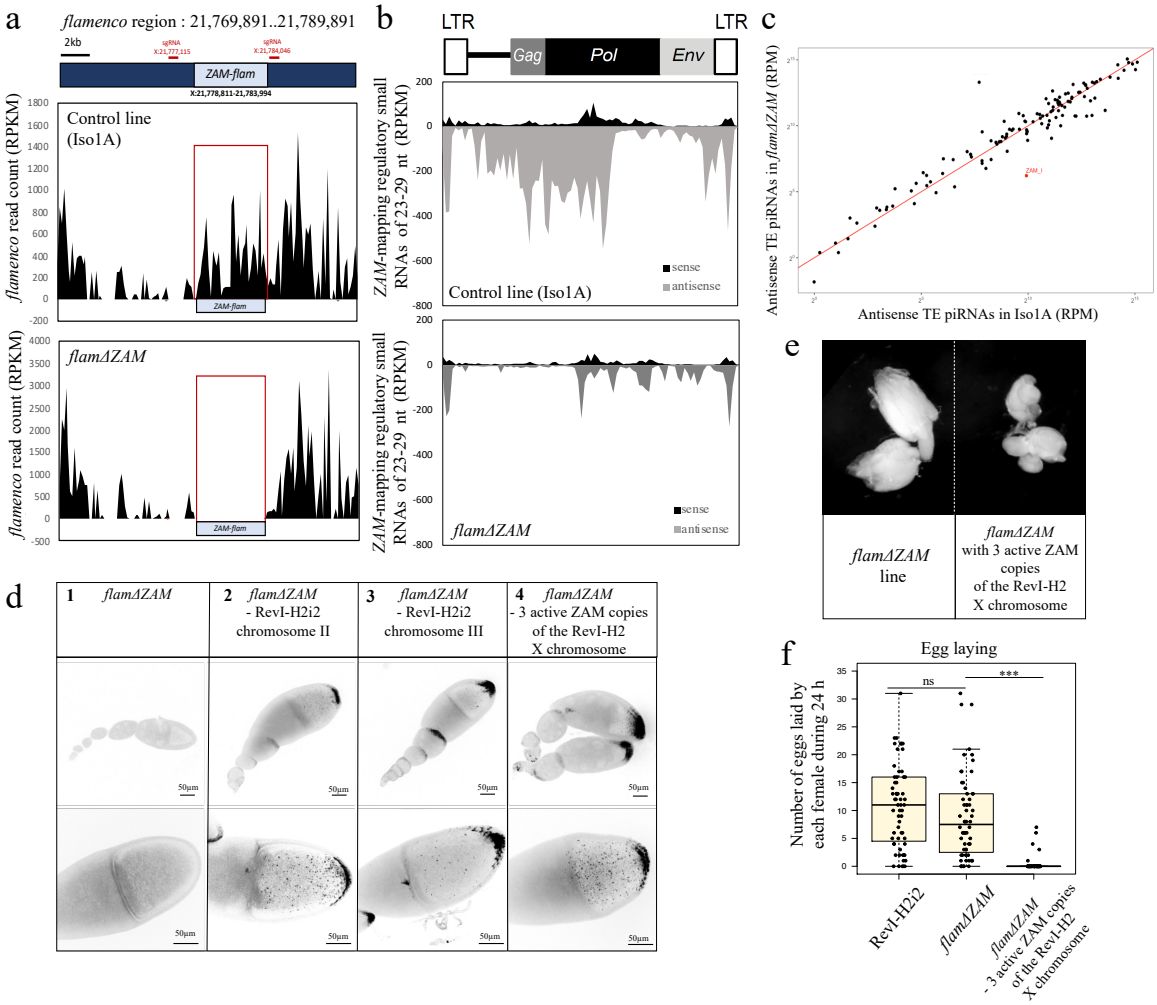

Figure 4: *ZAM* deletion from the *flamenco* piRNA cluster leads to *ZAM* reactivation and oocyte invasion.

a. Density plots showing genome-unique piRNAs mapping over 20 kb of the *flamenco* piRNA cluster (without mismatch) where the *ZAM* insertion is located (Release 6: X:21,769,891..21,789,891) in the control (Iso1A) and *flamΔZAM* lines. The position of the *flamenco ZAM* copy *(ZAM-flam)* is indicated. The positions of the sgRNAs used for *ZAM-flam* deletion by CRISPR-Cas9 are shown in red. **b.** Density plot of *ZAM*-mapping regulatory piRNAs along the *ZAM* sequence in control and *flamΔZAM* ovaries (up to 3 mismatches). **c.** Scatter plot showing the normalized counts of antisense regulatory piRNAs mapping to individual internal TE sequences in control ovaries (Iso1A) versus *flamΔZAM* ovaries. Antisense piRNA counts, mapped allowing up to 3 mismatches, were normalized per million of genome-mapping piRNAs (RPM, here in logarithmic scale). TEs in red have a *flamΔZAM*/*Iso1A* ratio <0.3. **d.** Color-inverted confocal images of ovarioles (upper panels) and stage 10 egg chambers (lower panels) from the indicated genotypes showing *ZAM* smRNA FISH signal. **e.** Ovaries of the *flamΔZAM* line and of the *flamΔZAM* line with three recent *ZAM* copies introduced by genetic crossing and X chromosome recombination with the RevI-H2 line. **f.** Box plot displaying the number of eggs laid per fly per day by RevI-H2i2, *flamΔZAM and flamΔZAM* females with three recent *ZAM* copies. Each dot represents an individual female. The midline indicates the median value, and the box shows the first and third quartile. Error bars indicate the SD. ****p-value* <0.001; ns, not-significant (*p-value* >0.05) (Mann-Whitney test).

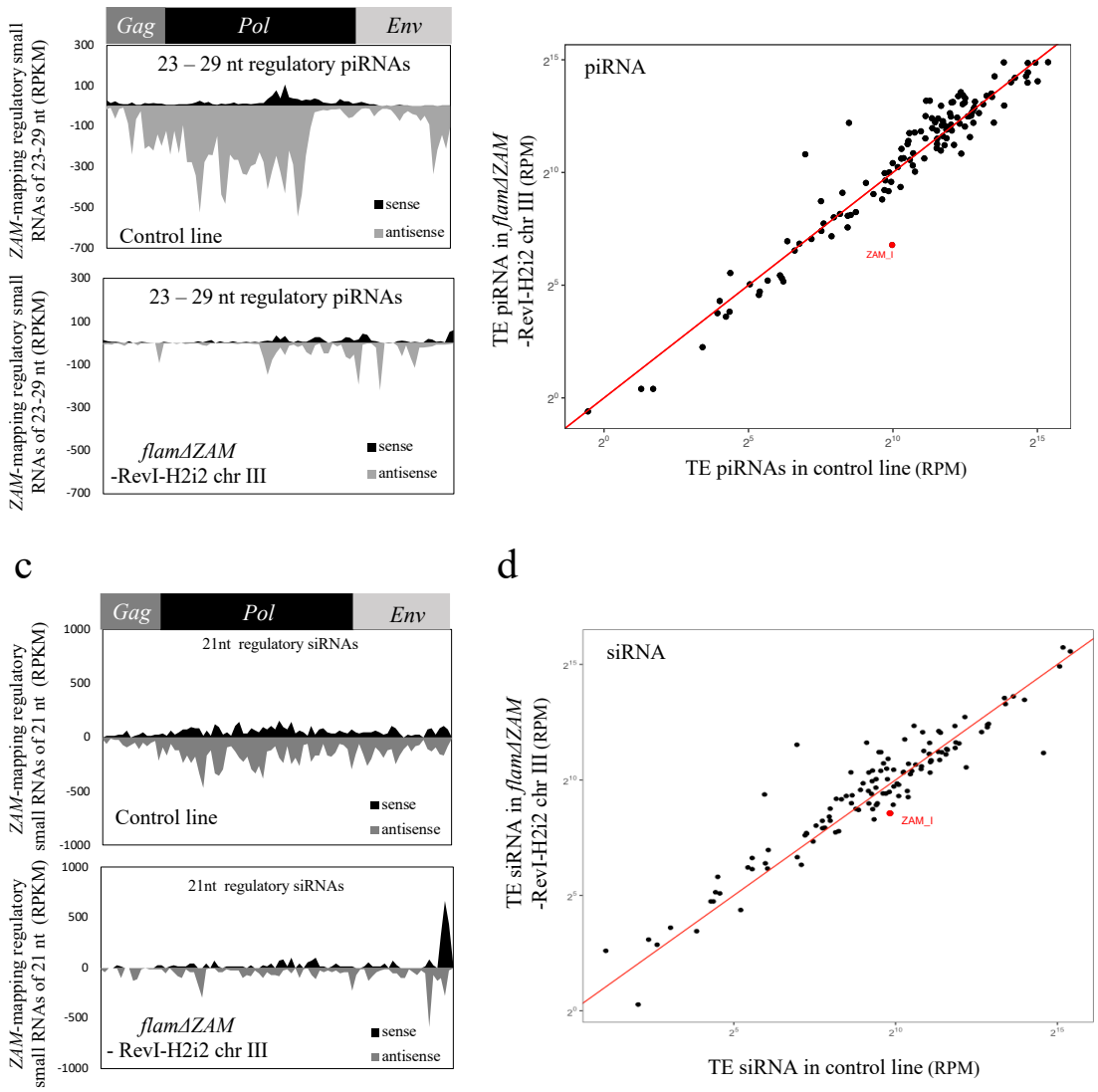

Figure 5: No initial piRNA and siRNA response after *ZAM* retrotransposon reactivation
a. Density plot of regulatory piRNAs along the *ZAM* internal sequence in ovaries from a control line (*white*-sKD) and from the *flamΔZAM*-RevI-H2i2 chr III line (up to 3 mismatches). **b.** Scatter plots showing the normalized counts of regulatory piRNAs mapping to individual internal TE sequences in control ovaries (*white-sKD*) versus *flamΔZAM*-RevI-H2i2 chr III ovaries. piRNA counts, mapped allowing up to 3 mismatches, were normalized per million of genome-mapping piRNAs (RPM, here in logarithmic scale). **c**. Density plot of *ZAM*-mapping regulatory siRNAs (21nt small-RNAs complexed with Argonaute proteins) along the *ZAM* internal sequence produced in control (*white*-sKD) and in *flamΔZAM* RevI-H2i2 chr III ovaries (0-1 mismatch). **d**. Scatter plot showing the normalized counts of antisense regulatory siRNAs mapping to individual internal TE sequences in control ovaries (*white-sKD*) versus *flamΔZAM* RevI-H2i2 chr III ovaries. Antisense siRNA counts, mapped allowing up to 1 mismatch, were normalized per million of genome-mapping siRNAs (RPM, here in logarithmic scale).

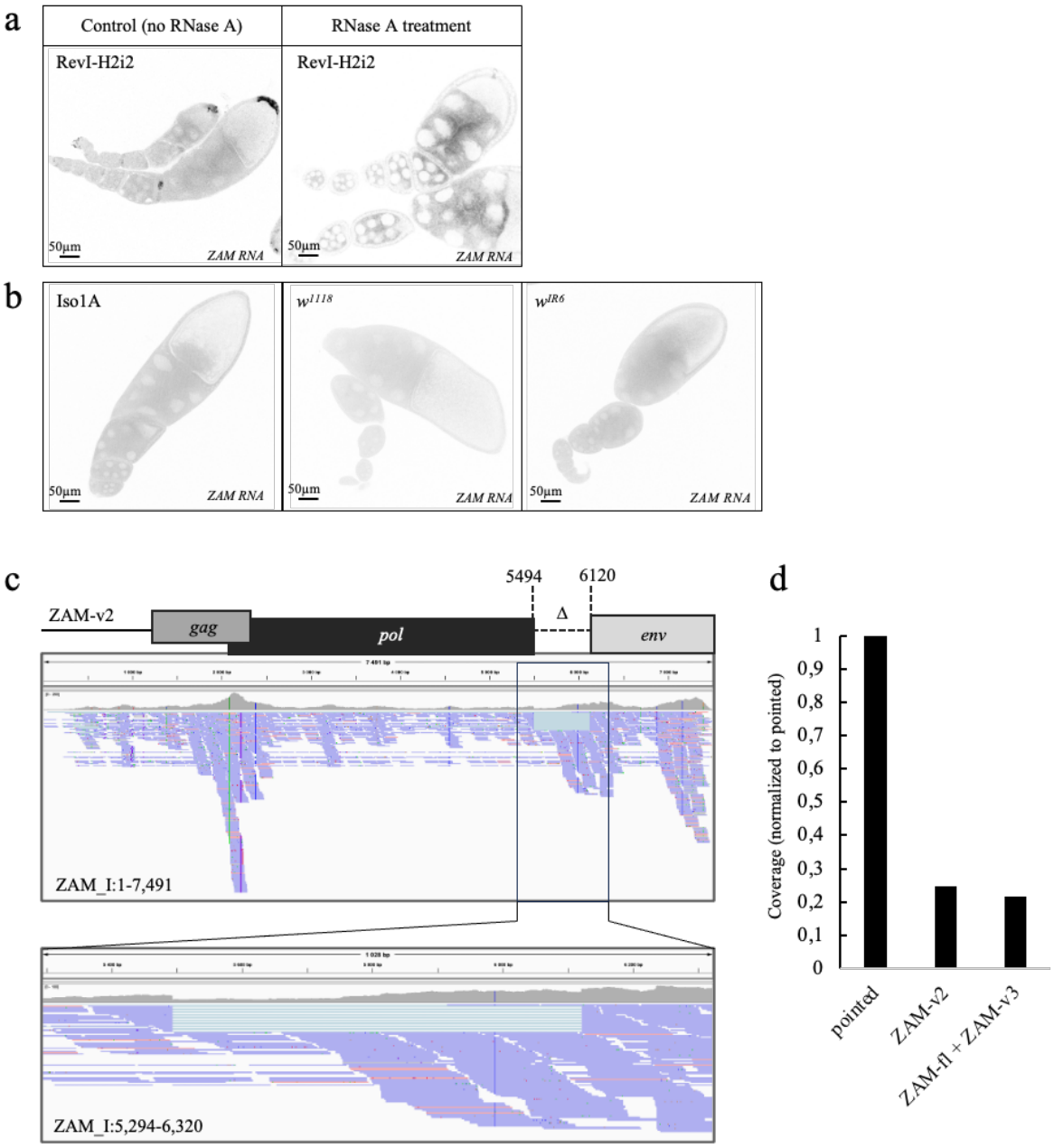

Supplementary Figure 1 (related to Figure 1)
a. Color-inverted confocal images of ovarioles from RevI-H2i2 ovaries showing *ZAM* RNA signal without (left panel) and after (right panel) RNase A treatment. **b.** Color-inverted confocal images of ovarioles showing that *ZAM* RNA is completely absent in Iso1A, w^{1118}, and w^{IR6} ovaries. **c.** Mapping of mRNA-Seq reads of the full-length *ZAM* (*ZAM-fl*) and of *ZAM-v2* to the reference *ZAM* internal sequences *ZAM*_I (Repbase) allowing splitting of the reads. Above is shown *ZAM-v2* structure. The inset below shows a zoom on the *ZAM-v2* deletion with the corresponding split reads. Reads corresponding to *ZAM* mRNA are in blue, antisense reads are in red. Positions of the shown regions within *ZAM*_I are indicated. d. Coverage of mRNA-seq reads corresponding to the indicated *ZAM*-variants normalized to the average coverage of the gene *pointed*.

1023

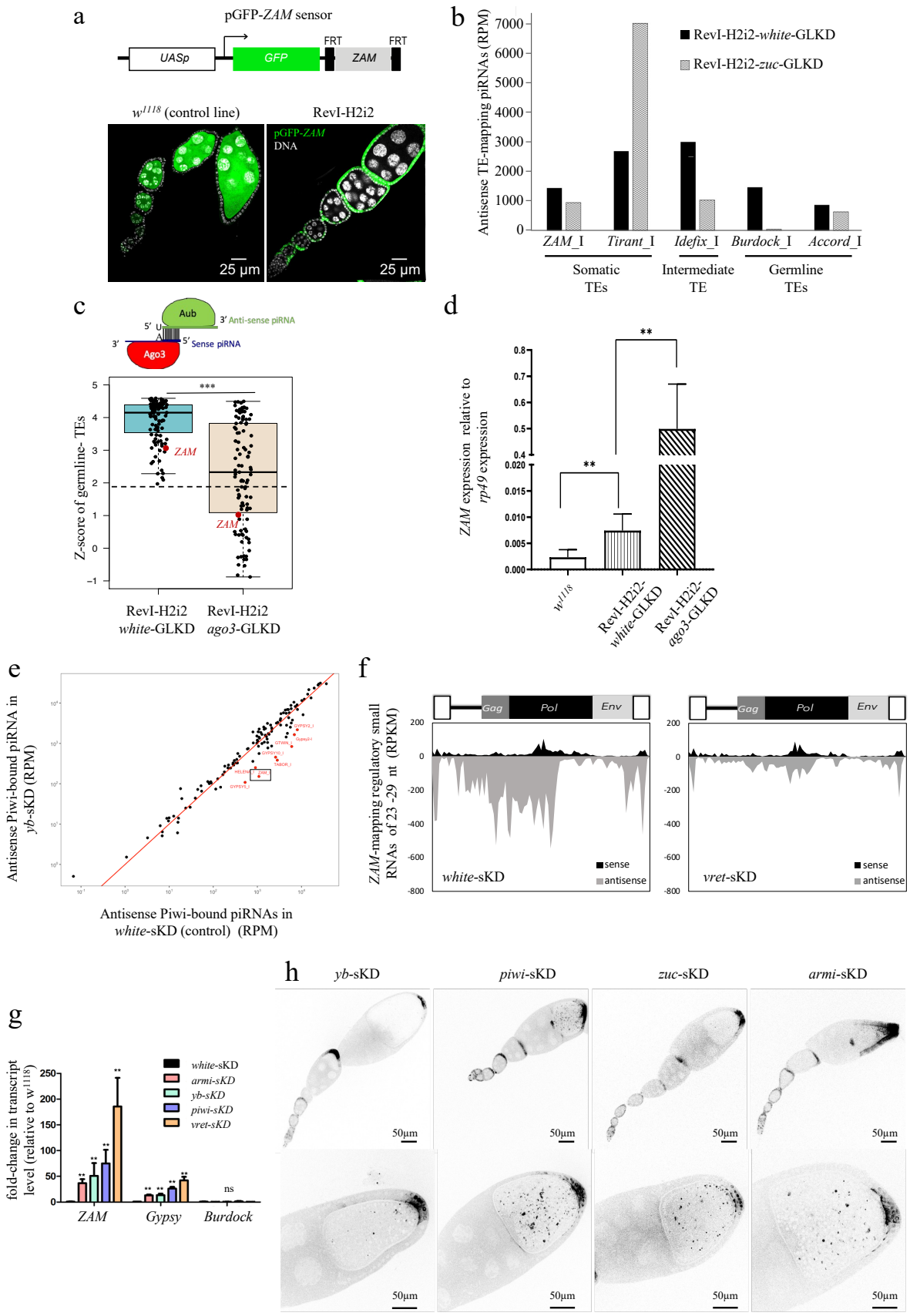

1024
1025
1026 **Supplementary Figure 2 (related to Figure 2)**

a. Confocal images of ovarioles with GFP (green) and DNA (white) staining. Ovarioles of the progeny of a cross between either w^{1118} control females or RevI-H2i2 females and males carrying the pGFP-*ZAM* sensor transgene driven by actin-Gal4. **b.** Antisense regulatory piRNAs (23-29 small-RNAs complexed with Argonaute proteins) mapping to TE internal sequences (0-3 mismatches) in the RevI-H2i2 line upon *white*- (control), or *zuc*-GLKD. Normalized per million of genome-mapping piRNAs. **c.** Box plot displaying the Z-score distribution of 10nt 5'-overlaps for TE-mapping piRNAs in the *white*-GLKD and *ago3*-GLKD RevI-H2i2 lines. Each dot represents a TE with a Z-score >1.96 (dotted line) in the control condition (*white*-GLKD). *ZAM* is highlighted in red. The midline indicates the median value, and the box shows the first and third quartile. Error bars indicate the SD. ****p-value* <0.001 (Mann-Whitney test). **d**. Bar plot showing the steady-state *ZAM* RNA levels in total RNA from ovaries with the indicated genotypes (RT-qPCR, normalized to *rp49*, primer sequences in Supplementary Table S5). At least three biological replicates and two technical replicates were used. ***p-value* <0.01 (Mann-Whitney tst); error bars indicate the SD. **e**. Scatter plot showing the normalized counts of antisense Piwi-bound piRNAs mapping to individual internal TE sequence in control ovaries (*white*-sKD) versus *yb*-sKD ovaries. Antisense piRNA counts, mapped allowing up to 3 mismatches, were normalized per million of genome-mapping piRNAs (RPM, here in logarithmic scale). TEs in blue have a *yb*-sKD/*white*-sKD ratio >3; TEs in red have a ratio <0.3. *ZAM* is boxed in black. **f.** Density plot along the *ZAM* sequence of *ZAM*-mapping regulatory piRNAs produced in *white*- and *vret*-sKD ovaries (up to 3 mismatches). **g**. Fold-change in the steady-state *ZAM, Gypsy* and *Burdock* RNA level for the indicated sKD ovaries, compared with *white*-sKD ovaries, measured by RT-qPCR (primer sequences in Supplementary Table S5). At least three biological replicates and two technical replicates were used. ***p-value* <0.01 (Mann-Whitney test); error bars indicate the SD. **h**. Color-inverted confocal images of ovarioles (upper panels) and stage 10 egg chambers (lower panels) from the indicated sKD lines showing *ZAM* RNA expression in follicle cells and in the ooplasm in indicated conditions.

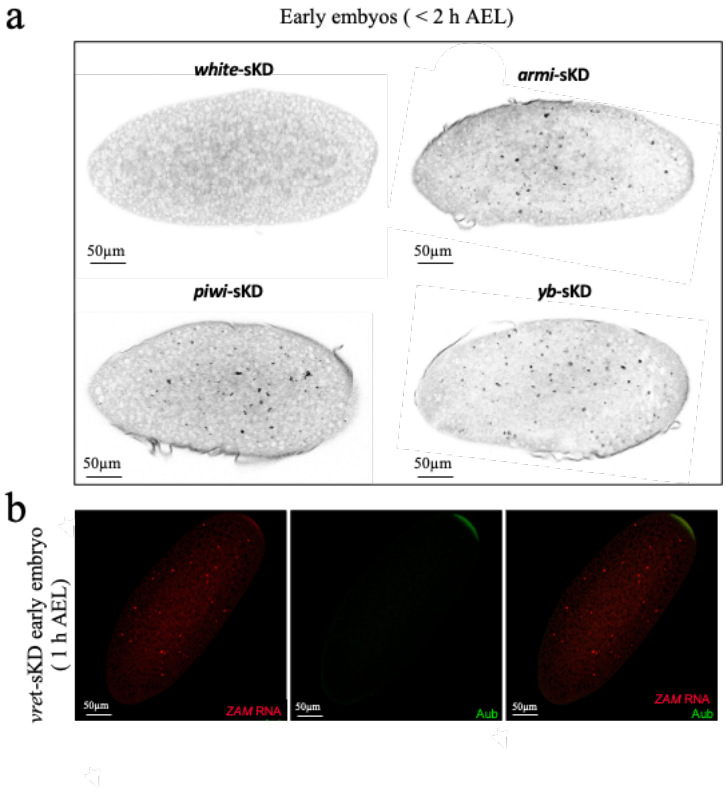

1055
1056
1057 **Supplementary Figure 3 (related to Figure 3):**
1058 **a.** Color-inverted confocal images of early embryos collected 0-2 hours after egg laying (AEL).
1059 Mothers harbor the indicated sKD of the piRNA pathway. *ZAM* RNA signal was detected by
1060 smRNA FISH. **b.** Projection of confocal images of stage 1 embryos (0-1 h AEL) laid by *vret*-
1061 sKD females showing *ZAM* RNA detected by smRNA FISH and Aub protein immunostaining.
1062 Both accumulated at the posterior pole of the embryo where future germ cells cellularize (Z-
1063 projection of 25 stacks).
1064
1065

1066

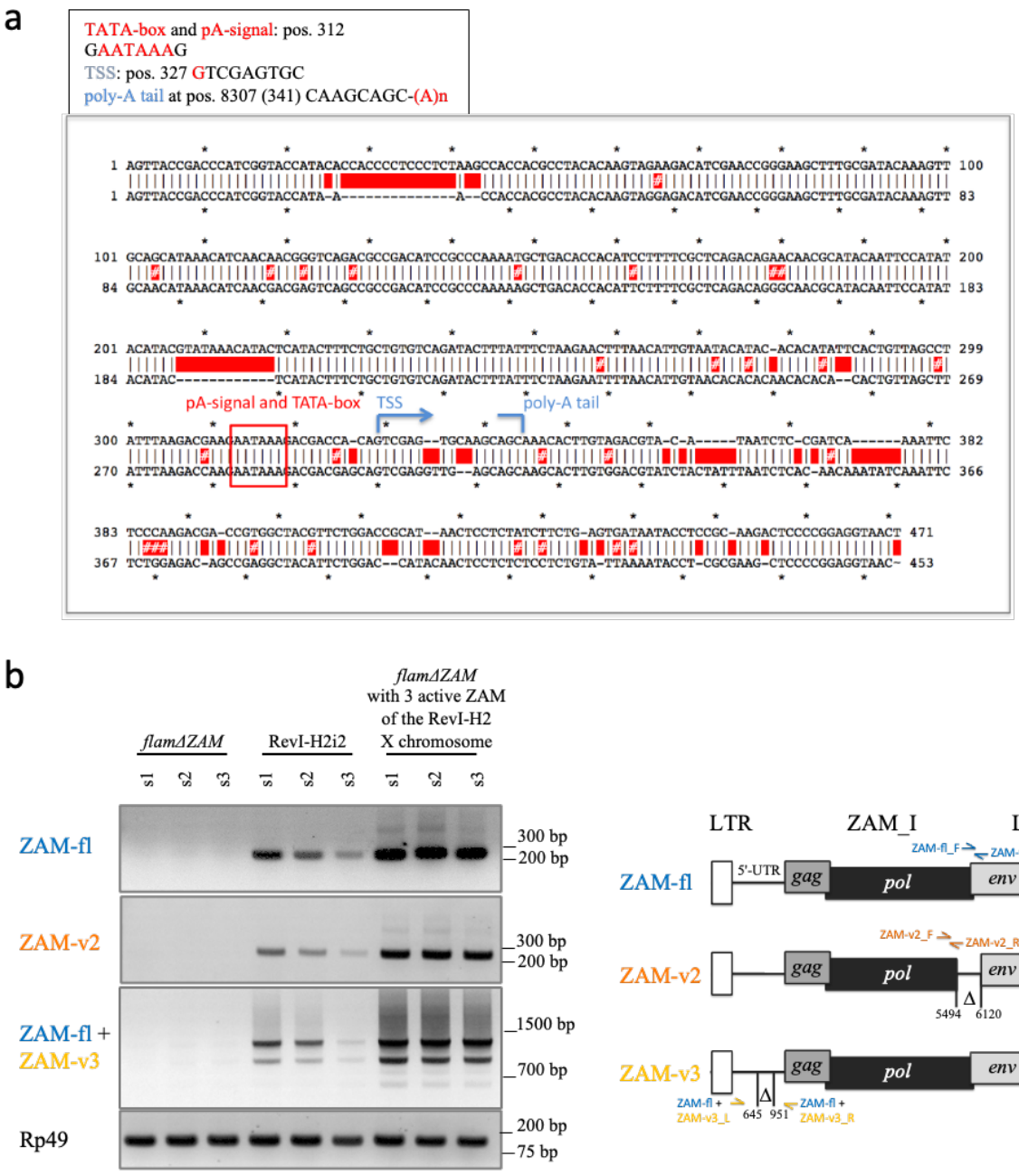

1067
1068
1069 **Supplementary Figure 4 (related to Figure 4):**
1070 **a.** Sequence alignment of the RevI-H2 consensus *ZAM* LTR and the *ZAM* solo-LTR that
1071 remains in the *flamΔZAM* line after CRISPR-Cas9 deletion of the internal *ZAM* sequence in
1072 *flamenco*. The image shows the RevI-H2 consensus *ZAM* LTR (upper sequence) and the *ZAM*
1073 solo-LTR (lower sequence) with their TATA-box and polyadenylation signal (pA-signal) at
1074 position 312 of the *ZAM* consensus, the transcription start site (TSS, at position 327), the start
1075 of the poly-A tail at position 341 (CAAGCAGC-(A)n), according to Leblanc et al, 1997. **b.** RT-
1076 PCR results showing the expression of the different *ZAM*-variants in the ovaries of the
1077 following fly lines: *flamΔZAM*, RevI-H2i2 and *flam*ΔZAM with three copies of *ZAM* from the
1078 RevI-H2 X chromosome (one *ZAM-fl*, one *ZAM-v2* and one *ZAM-v3*). Three biological
1079 replicates were used for each condition (s1, s2, s3). *Rp49* has been used as the housekeeping
1080 gene control. The primers used for specific amplification of each variant are indicated on the

1081 schematic representation of *ZAM* variants and represented by arrows, and color-coded as
1082 follows: Blue: Primers for specific amplification of *ZAM-fl*. Orange: Primers for specific
1083 amplification of *ZAM*-v2 (primer *ZAM*-v2_R overlaps left and right edges of the *ZAM*-v2
1084 deletion). Yellow: Primers for amplification of Z*AM-fl* and *ZAM*-v3, where the size of the
1085 amplification product differs due to a specific deletion in the 5'-UTR of *ZAM*-v3. (primer
1086 sequences in Supplementary Table S5).
1087
1088

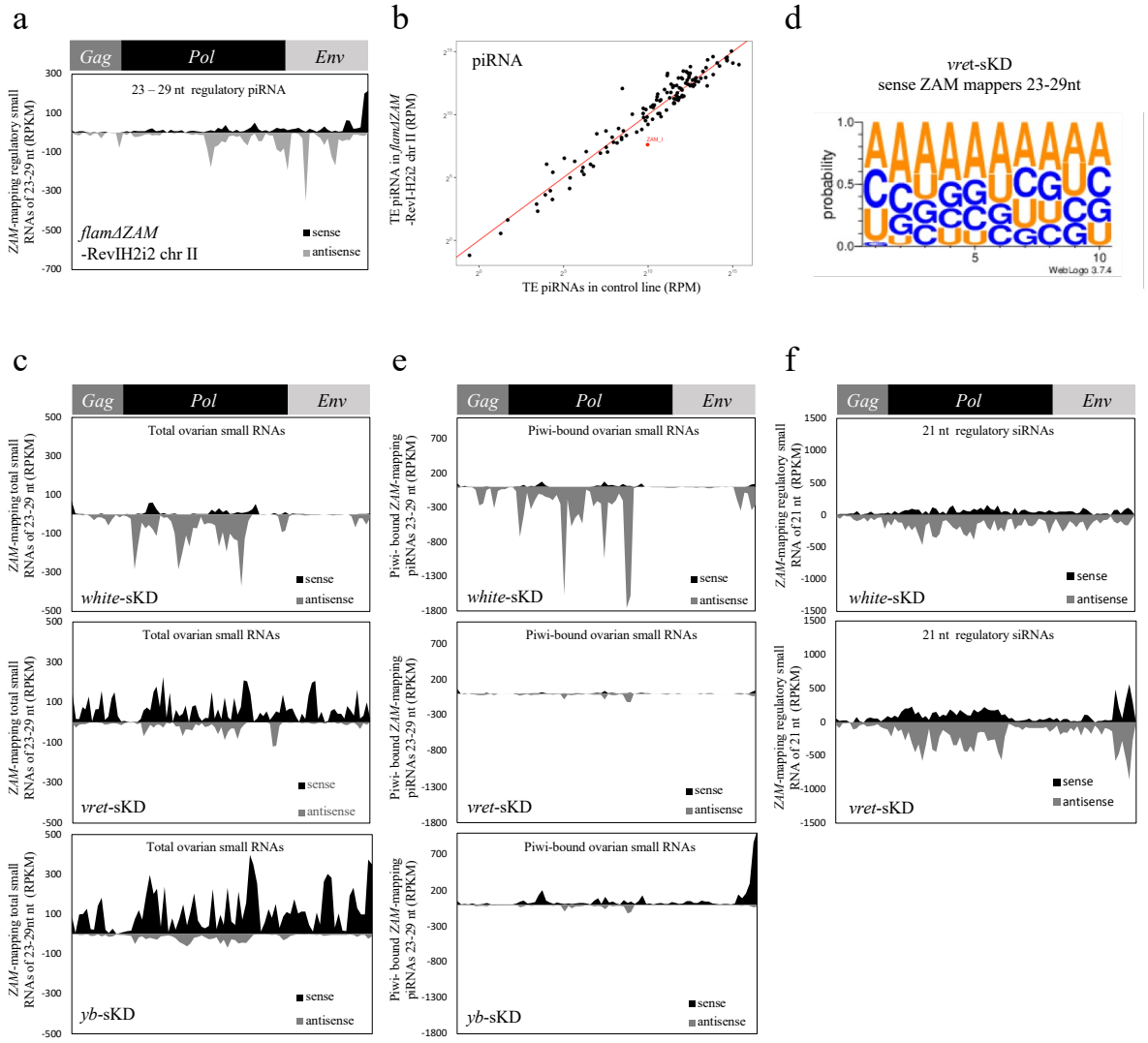

Supplementary Figure 5 (Related to Figure 5)

a. Density plot of *ZAM*-mapping regulatory piRNAs (23-29 nt small-RNAs complexed with Argonaute proteins) along the *ZAM* internal sequence in *flamΔZAM*-RevI-H2i2 chr II ovaries (up to 3 mismatches). **b.** Scatter plots showing the normalized counts of regulatory piRNAs mapping to individual internal TE sequences in control ovaries (*white*-sKD) versus *flamΔZAM*-RevI-H2i2 chr II ovaries. Antisense piRNA counts, mapped allowing up to 3 mismatches, were normalized per million of genome-mapping piRNAs (RPM, here in logarithmic scale). **(c)** Density plot of total small RNAs of 23 to 29 nt along the *ZAM* sequence in *white*-sKD, *vret*-sKD and *yb*-sKD ovaries (up to 3 mismatches). **c.** Density plot of total *ZAM*-mapping small RNAs of 23 to 29 nt along the *ZAM* internal sequence in *white*-sKD, *vret*-sKD and *yb*-sKD ovaries (up to 3 mismatches). **d**. Sequence logo for the first ten positions in ZAM-mapping sense small RNAs of 23 to 29nt (from total ovarian small RNA) in *vret*-sKD ovaries. The nucleotide height represents its relative frequency at that position. **e.** Density plot of *ZAM*-mapping Piwi-bound piRNAs along the *ZAM* internal sequence in *white*-sKD, *vret*-sKD and *yb*-sKD ovaries (up to 3 mismatches). **f.** Density plot of *ZAM*-mapping regulatory siRNAs (21nt small-RNAs complexed with Argonaute proteins) along the *ZAM* internal sequence produced in *white*-sKD and *vret*-sKD ovaries (0-1 mismatch).

M* = PBac{w[+mC]=PB}CG11583[c01124] P{ry[+t7.2]=neoFRT}80B
FM7a = Bar^{1} sc^{8} v^{Of} w^{a} y^{31d}
Pin = $\beta Tub60D^{Pin-1}$

Supplementary Figure 6

Description of the genetic crosses performed to obtain the different RevI-H2i2-GLKD lines.

1115
1116
1117 **Supplementary Video 1**
1118 Video of confocal Z-stacks overlay of stage 10 egg chambers from vret-sKD ovaries expressing
1119 Yolk-protein-1-GFP (green) showing ZAM smRNA FISH signal (red).
1120
1121

Supplementary Table S1 – ZAM insertions in the RevI-H2i2 genome

number	chromosome	insertion site (Release 6 genome)	orientation	type	locus	comment
1	X	X:1602129-1602133	minus	ZAM-v2	intron of the overlapping Mur-2B and broad genes	ZAM deleted for internal positions 5494-6120 (Repbase ZAM_I)
2	X	X:1980714-1980717	minus	ZAM-fl (full-length)	intron of gene Hr4	
3	X	X:19249375-19249375	minus	ZAM-v3	intron of gene His3st-B	ZAM deleted within the 5'-UTR, internal positions 645-951 (Repbase ZAM_I), inserted in a Jockey TE which is absent in the reference genome
4	X	X:22257753 or X:22373661	minus	ZAM-fl (full-length)	piRNA cluster 56 or 13 (George, Jensen et al., 2015)	
5	X	X:23212829	plus	ZAM-fl (full-length)	piRNA cluster 9 (X:23150001-23545000, George, Jensen et al., 2015)	
6	X	X:23368838-23368841	minus	ZAM-v2	piRNA cluster 9 (X:23150001-23545000, George, Jensen et al., 2015)	ZAM deleted for internal positions 5494-6120 (Repbase ZAM_I)
7	X	X:23513106-23513113	minus	ZAM-v2	piRNA cluster 9 (X:23150001-23545000, George, Jensen et al., 2015)	ZAM deleted for internal positions 5494-6120 (Repbase ZAM_I)
8	2L	2L:8158963-8158966	plus	ZAM-fl (full-length)	intron of gene PAPLA1	inserted in a NOMAD TE which is absent in the reference genome
9	2L	2L:15773891-15773894	plus	ZAM-fl (full-length)	intergenic region	
10	2R	2R:1808663-1817084	plus	ZAM-fl (full-length)	intergenic region	ZAM copy also present in the reference genome Release 6
11	2R	2R:6793620-6793623	plus	ZAM with an internal deletion	intron of gene Epac	ZAM deleted for internal positions 2332-5754 (Repbase ZAM_I)
12	2R	2R:11601808-11601811	minus	ZAM-v3	intron of gene toutatis	
13	3L	3L:4299131-4299137	minus	ZAM-v1	intron of gene dyl	ZAM deleted for the 5'-UTR, internal positions 60-1218 (Repbase ZAM_I)
14	3L	3L:19980882-19980883	minus	ZAM with internal deletions	intergenic region	ZAM deleted for internal positions 13-2993 and 5494-6120 (Repbase ZAM_I)
15	3R	3R:12079947-12079950	plus	ZAM-v2	intron of gene ATP8B	ZAM deleted for internal positions 5494-6120 (Repbase ZAM_I)
16	unknown	NW_007931121.1:45136-45142	plus	ZAM-fl (full-length)	rDNA	
17	unknown	possibly close to X:23239427	(plus)	ZAM with internal deletions	possibly piRNA cluster 9 (X:23150001-23545000, George, Jensen et al., 2015)	ZAM deleted for internal positions 2332-5754 and 6116-7265 (Repbase ZAM_I)
18	unknown	NW_001845412.1:1075-1078	minus	ZAM with an internal deletion	unknown	ZAM deleted for internal positions 2929-5615 (Repbase ZAM_I)

1122
1123

Supplementary Table 2 – Drosophila lines used

Category	*Gene name*	*CG_Number*	*Stock number*	*Genotype*	*Source*	*Notes*
RNAi line	white	CG2759	BDSC_35573	y[1] sc[*] v[1] sev[21]; P{y[+t7.7] v[+t1.8]=TRiP.GL00094}attP2	Bloomington	
RNAi line	armitage	CG11513	BDSC_34789	y[1] sc[*] v[1] sev[21]; P{y[+t7.7] v[+t1.8]=TRiP.HMS00098}attP2	Bloomington	
RNAi line	yb	CG6272	VDRC_110056	P{KK105851}VIE-260B	VDRC	
RNAi line	piwi	CG6122	BDSC_37483	y[1] sc[*] v[1] sev[21]; P{y[+t7.7] v[+t1.8]=TRiP.GL00626}attP40	Bloomington	
RNAi line	vreteno	CG4771	VDRC_34897	w1118; P{GD11424}v34897	VDRC	
RNAi line	zucchini	CG12314	BDSC_35227	y[1] sc[*] v[1] sev[21]; P{y[+t7.7] v[+t1.8]=TRiP.GL00111}attP2	Bloomington	
RNAi line	argonaute 3	CG40300		y[1] sc[*] v[1] sev[21]; P{y[+t7.7] v[+t1.8]=TRiP.GL00117}attP2	Bloomington	
RNAi line	aubergine	CG6137	BDSC_35201	y[1] sc[*] v[1] sev[21]; P{y[+t7.7] v[+t1.8]=TRiP.GL00076}attP2	Bloomington	
white mutant, otherwise wild-type	white		BDSC_3605	w[1118]	Bloomington	
nanos-Gal4 driver			BDSC_4937	w[1118]; P{w[+mC]=GAL4::VP16-nos.UTR}CG6325[MVD1]	Bloomington	
traffic-jam-Gal4 driver				w; tj-Gal4/CyO	Unknown	
RevI-H2i1					Produced in the lab	Isogenic line derived from the RevI-H2 stock
RevI-H2i2					Produced in the lab	Isogenic line derived from the RevI-H2 stock
RevI-H2i3					Produced in the lab	Isogenic line derived from the RevI-H2 stock
RevI-H2i4					Produced in the lab	Isogenic line derived from the RevI-H2 stock

1124
1125
1126
1127

Supplementary Table 3 – smRNA FISH probes

Oligo number	ZAM (this paper) 5'- 3'	Burdock (from Senti and al,.2015) 5' - 3'
1	GAAAAAGAAATGTTGGCAAT	AGGTTATCACTGTCACTCAT
2	AATATGGGCAGTAAAATACT	GCTTGACACTAGGTTGTCTA
3	AGACCATATATTTATGGCGT	TGGTGCGCTGACCATTTATT
4	TACAGATCACAAGCCACTAA	TTTTTTCTGCACTGTTTTGC
5	TGAATTTCAAAGAACCCAAC	CCACCAATTATCTGATGACT
6	AAAAATAATTCGTTGGAGAC	CGCTAGTTGTCTTTGTTTTT
7	TCCAACTCATGGAATACAAT	AACTGAGCTTCAAATTCCAT
8	TCACAAGAAAGGTTCACAAA	AACAGCACTCTCTACGATCG
9	TGTAATTGCAGACGCCTTAA	TGATTGTTTTTGGACTGCGA
10	GTAGAGCGGACCCAAATTTA	TCATTCATCTCCTGCAATTG
11	AACTACAACGAAACACTGAC	GGTGTTCACTGTTAATTTCC
12	TGTTAAGCCTTGCCCCACAT	CTACATAAGTTTCCACCTCT
13	CCGAAAAACCTATTAACGAA	TATATCTAGAGGCTCGCTAC
14	AACACGCAACTCATACTAGA	GCCATCAAAATCTGGCAGAG
15	TCTTACCAAACTACAACACC	CTTCCCTCGTAATCTTTGAA
16	AGGAAAAAATATTCACAGCC	CCAAGAGCTTGGTAAAATGT
17	AAAATCTTGAAAGGAACCCT	AAGCCAATACTGTATTCGCT
18	AAAACCTAACAGGATTTGCG	GCTTTGAAATGTAACGGAGT
19	CATTCTTGGCGGACGATAAT	TGTGAAATCAAGACGGCTGA
20	TCCGCATTAATCGAAAAAGC	TAGATAGATCGGCCTTTTGT
21	TTCTCCACGAAATCGTAGGA	GTCGCAAAGTTGATAGCTCT
22	ACCCCGAACAAAACAAATTC	TCAGTAAGAGTCATGTCTCC
23	GGAATATCACACTAACAGCA	TCTTGTTGGTAAGTAGGGTC
24	GAGGCATAGACGAAACATTC	GCCAAGGCACTATCAAATGT
25	TTCACCTCAAACGAGAAACC	GTCCTGTACTTTTCATTCAG
26	ACTTCCCCAATATGAAAAAC	CTCCGGTTACAAATACACGT
27	AATTAGGAATTGCGAAACCT	ATGTCGCTCAACGATTTCTT
28	GTCTAAAACTCAAATACGAC	ATCTTTTGGACCTTTTGCAA
29	AGGCAACCACAAAATATAGT	TGGTTCGACTCGACCTCTTG
30	ATTTGAAACCCCAGAAACCC	AAGGGCGAATTGGTAACGCT
31	GAAACCCCTCGACATAATAC	CCCTGTCTCCAATATTTTTA
32	ACCTGACAATCATAGACAAA	TGCCTTTGTTCGATTTTCTG
33	TCTCAAAATTCGCAGCTGTC	TGAGTTTCTATCCTTATCGC
34	TACCCCATCCCAAATAGAAA	TTTTTAGTTTGCATGGGCAT
35	CGGCATCAATTGCATCAAAG	CACCTGACGCTTGCTAAAAT
36	TTCAGTCAATTCGGACTACC	GGATTTGTTAACTGGACTGG
37	CAAAAAACTAATACACGACC	TTCTTCTAGATCGCATGGAT
38	AGGAGTAGAATTTTGCAACG	GGAGTTTGTCCAAAATTTCC
39	CCATGTCACATCCTTCCAGC	AATATTTCCCTGAGTCGGAA
40	AGTAATTCTCCAGTAGAACG	GGTTGCGATGCGAATTGATT
41	ACACTCCTCTTTGACAGAGA	CTGACTTGTGTTTTGCTGTT
42	AATACTAGACACACGGAAAA	TTGCGCATACCCAAAATGTC
43	ACACAAATTACCTACAGACC	CACTCGTTGGTCTTTTTGAT
44	ACGAAGAAATAATGTCAGAA	TTTTGGCCCTGTAAACCTTG
45	ATAACAACGCAATCCACTCC	GGTAAGTAGTTGATCCTCTG
46	CCACCAAACACACCCCTTTT	CTCACATTGACCTTTCTCAT
47	TGGTAGGACCCATTTATTCG	CCTTTTGATAACCGTCTGTA
48	ATACCCAATAATGAGCATGA	ATAATCATCAACCTCCGCTT

Supplementary Table 4 – Antibodies used

Antibody	Source	Dilution	Fluorochrome	Species	Reference
Primary antibody					
Goat anti-GFP	abcam	1/1000		Goat	ab5450
Rabbit anti-Aubergine	Homemade (Eurogentec) - polyclonal antibody	1/1000		Rabbit	
Rabbit anti-Gag-ZAM	Homemade	1/100		Rabbit	
Rabbit anti Env-ZAM	Homemade	1/1000		Rabit	
Secondary antibody					
Alexa Fluor 488 donkey anti-goat IgG (H+L)	Invitrogen (Fisher)	1/1000	Alexa 488	goat	A11055
Donkey anti-rabbit Alexa 488 IgG (H+L) 2mg/ml	life tech	1/1000	Alexa 488	rabbit	A21206
Goat anti-rat Cy3	Jackson Immunoresearch	1/1000	Cy3	rat	112-165-143
Fluorescent dyes					
DAPI	Sigma	1/500			D8417-1MG

Supplementary Table S5 - Primers used

	Name	Sequence	Used for
Rp49	rp49_R	AAACGCGGTTCTGCATGAG	RT-qPCR
	rp49_F	GACGCTTCAAGGGACAGTATCTG	
Burdock	Burdock_F	GGACAAACTCCATTTCCGACTC	RT-qPCR
	Burdock_R	TCCCTGAGCCTGACTTGTGT	
Gypsy	Gypsy-F	CGCTCGAAGGTTACCAGGTAGGTTC	RT-qPCR
	Gypsy_R	CTTCACGTTCTGCGAGCGGTCT	
ZAM	Zam_env_F	CTCCCAATCATCTCCTCCAA	RT-qPCR
	Zam_env_R	AGAAGTCGGGGTGCTCTTCT	
flamenco ZAM	ZAM-FLAM_F	TCGCTTAGGAGGGTAGCTTG	CRISPR SCREEN
	ZAM-FLAM_R	CTTAACACCTACTGTCAGTGC	
ZAM-fl	662_ZAMflRev_6360_F	CCTGCATTCCAGATCTTGCC	RT-PCR
	663_ZAMflRev_6587_R	ATTGATATAGAATCGGTGAGTG	
ZAM-v2	666_ZAMv2Rev_5752_F	GAATTTTGCAACGACATATTTCGA	RT-PCR
	667_ZAMv2Rev_5988_R	AGCATTTAGTATTGATATAGTATTACAG	
ZAM-fl + ZAM-v3	668_ZAMflRev_697_F	TAACCGCGAAACATGATATGC	RT-PCR
	669_ZAMflRev_1835_R	GTGTGTGATTCTAACACGGAG	

Supplementary Table S6 – small-RNA seq

Small RNA seq
TrapR sRNA from RevI-H2i1
TrapR sRNA from RevI-H2i2
TrapR sRNA from RevI-H2i3
TrapR sRNA from RevI-H2i4
Total RNA from RevI-H2i2- nos-Gal4- driven dsRNA-white
Total RNA from RevI-H2i2- nos-Gal4- driven dsRNA-Ago3
Total RNA from RevI-H2i2- nos-Gal4- driven dsRNA-Piwi
TrapR sRNA- from RevI-H2i2- nos-Gal4- driven dsRNA-Zuc
TrapR sRNA- from RevI-H2i2- nos-Gal4- driven dsRNA-white
TrapR sRNA from tj-Gal4-driven dsRNA-Vret
TrapR sRNA from tj-Gal4-driven dsRNA-white
TrapR sRNA from CRISPR flamΔZAM
Total RNA from tj-Gal4-driven dsRNA-Vret
Total RNA from tj-Gal4-driven dsRNA-white
Total RNA from tj-Gal4-driven dsRNA-yb